UNIVERSITY OF LATVIA

Summary of Doctoral Thesis

Mikus Milgrāvis

COMBINATION OF MAGNETIC FIELD INTERACTIONS FOR METALLURGICAL APPLICATIONS

Riga 2023

UNIVERSITY OF LATVIA

FACULTY OF PHYSICS, MATHEMATICS AND OPTOMETRY

Mikus Milgrāvis

COMBINATION OF MAGNETIC FIELD INTERACTIONS FOR METALLURGICAL APPLICATIONS

SUMMARY OF DOCTORAL THESIS

Submitted for the degree of Doctor of physics and astronomy
Subfield: fluid and gas mechanics

Riga 2023

The doctoral thesis was carried out at Faculty of Physics, Mathematics and Optometry University of Latvia and Institute of Physics University of Latvia from 2018 to 2022.

The thesis contains the introduction, three chapters, summary, and reference list.

Form of the thesis: collection of research papers in field of physics and astronomy, subfield of fluid and gas mechanics.

Supervisor: *Dr. phys.* **Andris Bojarevičs**.

Reviewers:

1) *Dr. phys.* **Guntars Kitenbergs**, University of Latvia;
2) *Dr.* **Egbert Baake**, Leibniz University Hannover, Germany;
3) *Dr.* **Andrew Kao**, University of Greenwich, Great Britain.

The thesis will be defended at the public session of the Doctoral Committee of field of physics and astronomy, University of Latvia, on 26th of May, 2023.

The thesis is available at the Library of the University of Latvia, Raiņa bulvaris 19.

Chairman of the Doctoral Committee _____ **Andrejs Cēbers**

Secretary of the Doctoral Committee _____ **Sintija Siliņa**

ISBN 978-9934-18-966-1
ISBN 978-9934-18-967-8 (PDF)

Abstract

Static and alternating magnetic field interaction with liquid metal is widely used in industry, while the interaction of magnetic field combinations has been studied insufficiently, especially in tasks of practical importance. This study investigates how to use combination of magnetic fields for three different practical applications.

1. This work proposes to improve the metallurgical silicon purification process by increasing the surface area of liquid silicon. By using electromagnetically induced surface waves, more efficient removal of impurities is proposed. By using a physical model, the study shows the formation of waves in crucibles with various diameters and depending on applied alternating and static magnetic field. Study also shows the generated surface wave amplitude limits, as well as developed laboratory prototype for the excitation of waves on the surface of liquid silicon.

2. The new concept electromagnetic method for mixing particles into an alloy to obtain metal matrix composites is developed. Permanent magnet rotor technology for liquid aluminum stirring was developed. The stirrer technology is adapted for mixing micro and nano particles into the alloys. The research shows that by using the developed permanent magnet stirrer in combination with induction heating, particles can be mixed into aluminum alloys and the composite can be obtained in a non-contact manner.

3. Electromagnetically generated cavitation in liquid metal is studied in order to disperse particle agglomerates in the metal matrix composites. The developed method is studied as a contactless alternative to the mechanical sound excitation in the melt. Cavitation effect is induced in the melt by using combined alternating and static magnetic field. Sample analysis show improvement in particle distribution. The developed method was further developed by studying influence of pulsed magnetic field on particle distribution in metal matrix composites. The work concludes with the study of a continuous casting crystallizer, which is developed for the future production of metal matrix composite rods.

Both proposed applications for production of metal matrix composites have shown promising results and are being developed further.

Contents

General description

Introduction

Historically, the development of metallurgical processes has directly influenced the development of society and has become one of the main branches of industry. Electromagnetic (EM) methods in modern metallurgy are considered to be one of the most promising for improvement of production processes, so research in this topic is important for the overall development of the industry. The processing of liquid metal with mechanical methods during its production is difficult due to hot and aggressive environment, which results in accelerated wear of parts, heat loss and important safety aspects. With electromagnetic methods, processing is conducted in a contactless manner, gaining advantages in all the mentioned aspects.

In metallurgy, EM methods are used for liquid metal transport, stirring, heating, flow measurement, and other applications. For such applications inductor systems are mainly used [1,2]. Permanent magnets are becoming more accessible, so rotating permanent magnet systems are increasingly introduced for similar applications. The main advantage of magnets is that for magnetic field generation no current generators are needed [3–5].

Combinations of magnetic fields (m.f.) are rarely used and examined in industrial applications and even in research, while the achieved regimes can be unique and have new practical applications [6–8].

Conducted research in this dissertation focuses on combined magnetic field interactions for practical applications in metallurgy, including the studies of the necessary m.f. combinations for the relevant tasks, as well as developing the technical solutions required for practical and efficient implementation of combined m.f. The development of unique experimental systems is also an essential part for the implementation of experiments, which includes the creation of inductors and permanent magnet systems according to the specifics of the research.

The thesis explores combined magnetic field applications for improvement of three technological processes or in three research subfields. Overall, this thesis is described in seven scientific publications [dis1-dis7]. Research subfields are categorized as follows:

1. Electromagnetic excitation of surface waves on the liquid metal for surface area increasement purposes, described in Chapter 1 of this summary. The method for surface area increasement has potential to improve the metallurgical silicon purification process. Surface waves induced by a low-frequency alternating magnetic field have been extensively studied in the SIMAP laboratory, where wave formation and excitation was presented analytically and demonstrated experimentally with liquid mercury [9–11]. By increasing the alternating magnetic field frequency or by increasing the diameter of the crucible,

the system begins to be significantly affected by the skin-effect, which limits the formation of waves over the entire melt surface. Surface deformations caused by an alternating magnetic field can be both amplified and damped by a static magnetic field. Research is mostly carried out with aim to suppress and control the surface deformations caused by the alternating field, because the deformations negatively affect other metallurgical processes [12,13]. In this thesis, it is proposed to use combined static magnetic field (B_{DC}) and alternating magnetic field (B_{AC}) in order to induce waves over the entire melt surface even in cases where the system is strongly affected by the skin-effect. For modeling experiment for surface wave studies Galinstan is used. Galinstan is metal liquid at room temperature. The work consists of, firstly, the development of the experimental system [dis1], including a new type of inductor for B_{AC} generation and a permanent magnet system. Secondly, the results from electromagnetically excited surface wave [dis2]. Thirdly, the technology is developed for a laboratory prototype for surface wave excitation on silicon melt surface, reaching the 4th technology readiness level (TRL 4) [14].

2. As a second research subfield is particle mixing into the melt for production of metal matrix composites by using electromagnetic methods, described in Chapter 2. Metal matrix composites (MMC) is a new and rapidly growing sub-field of metallurgy. MMC is a material that consists of metal with particles mixed into it, thus obtaining a composite material with improved mechanical, thermal and other properties. For example, aluminum matrix composites (AMC) can have improved tensile strength by more than 30% comparing to base alloy [15–17]. Powder metallurgy is one of the most widely used MMC production methods [18,19], however it is essential to continue development of MMC production through metallurgical route, thus making production efficient and scalable. Currently, the stir-casting method [20–23], in which particles are mixed into the metal with a rotating blade, is considered as one of the most promising methods in AMC metallurgical production. The method is effective, but is not designed for large production volumes, and because of mechanical mixing, there are material losses and the blade erosion. As a solution, the studies suggest replacing the rotating blade with an electromagnetic stirrer [24,25], where the flow of liquid metal is initiated by inductor system. These stirrers work similar as the induction stirrers used in metallurgy for aluminum furnaces [1]. Studies in Institute of Physics of the University of Latvia has shown that a similar flow can also be generated by rotating permanent magnet dipole. Comparing to inductor systems, the permanent magnet system does not require specific cooling and powerful transformers [26]. In this study a permanent magnet stirrer technology has been developed to industrial scale and tested in a factory on a 20-ton aluminum furnace [dis3]. Then, the permanent magnet stirring method was adapted to mix particles into aluminum melt and a series of experiments with different aluminum

alloys and particles were performed [dis4]. As a result, a combined permanent magnet stirrer and induction heating method for mixing particles in aluminum alloys has been developed.

3. The third research subfield is dispersion of particle agglomerates in metal matrix composites. Research described in Chapter 3. Although metallurgical methods for particle mixing into the alloy are widely used, often the distribution in the melt volume is not uniform [27]. Particles in metal matrix composites tend to form agglomerates, which leads to unequal material properties. It has been shown that as the particle characteristic size decreases, the improvement in the mechanical properties of the material increases. At the same time, nanoparticle dispersion in metal matrix composites is technically challenging [18,28]. Mechanical sound excitation in the metal is often used in MMC production to disperse particle agglomerates. As a result of intense pressure oscillations generated by a mechanical probe (sonotrode), cavitation in the melt is initiated. Cavitation is considered as a main mechanism for particle agglomerate dispersion [17,29]. This work investigates initiation of similar pressure fluctuations using electromagnetic methods to obtain particle dispersion in MMC material in a non-contact manner. Advantage also could be that particle dispersion is performed faster and can be adapted larger volumes. Electromagnetic cavitation generation has been studied by Vives [30], while Grant [31] has proposed to improve particle distribution in ODS steels by inducing cavitation with a combined B_{AC} and B_{DC} magnetic field. Since the cavitation threshold is affected by alloy composition and other system parameters, the required EM field parameters in aluminum alloys are unclear. In order to determine the parameters of the electromagnetic field at which metal cavitation begins and to study whether such exposure affects the distribution of particles, a combined B_{AC} and B_{DC} magnetic field impact on aluminum and tin alloy samples with particles were studied [dis5]. The intensity of the BAC and BDC fields at which cavitation effect was observed would be impossible to realize in an industrial scale, therefore a concept of pulsed (PMF) and static magnetic field instead of B_{AC} and B_{DC} was proposed. The effect of PMF has been widely studied for grain refinement during the crystallization of aluminum alloys. Such treatment during crystallization improves the tensile strength and other properties of the alloy [32–34]. The effect of PMF on the production of metal matrix composites has been studied by synthesizing particles in the alloy (in-situ method) [35], but the effect of PMF on the particles mixed into the alloy has not been studied so far. The effect of combined PMF and BDC on the grain structure in a tin-lead alloy was studied by Hua [6] – the study mainly focused on improvement of alloy microstructure, but the physical processes of magnetohydrodynamics (MHD) were not described. During thesis [dis6] a combined interaction of PMF and B_{DC} fields was developed. The method allows to develop high-intensity pressure oscillations into the melt up to 7 times per

second. Impact of the developed method on Sn-Pb alloy microstructure and TiB_2 particle distribution in aluminum 6061 alloy was studied. In order to use the developed MMC material as an alloying alloy or material for 3D printing, it is necessary to cast alloy in rods. Crystallization of the alloy in combination with electromagnetic stirring allows to obtain a material without pores and homogeneous, fine-grained microstructure [36,37]. To crystallize the alloy, a continuous casting crystallizer to obtain 12-20mm diameter rods has been developed. This work is presented in article [dis7]. In order to obtain a homogeneous fine-grained alloy structure, electromagnetic stirring of the alloy is carried out in the crystallization zone, which is created by a permanent magnetic field interacting with a current flowing parallel to the direction of crystallization. Currently, the EM interaction is studied for microstructure refinement during aluminium alloy casting, but in the future it is planned to crystallize the obtained metal matrix composite. The goal is to develop and study the full production cycle of MMC.

Aim and tasks of the thesis

Aim of this thesis is to study the potential applications of combined magnetic field in metallurgical processes.

Following **tasks** are set:

1. Study the excitation of surface waves on the surface of a liquid metal using combined magnetic fields.
2. Develop a method for electromagnetic mixing of non-magnetic micro and nano particles into liquid metal.
3. Develop a combined electromagnetic method for particle dispersion in metal matrix composites.

List of publications and conferences

Scientific publications included in this thesis

Publications about electromagnetically generated surface waves:

[dis1] **M. Milgrāvis**, A. Bojarevičs, A. Gaile, V. Geža, The Design of a System to Compose 50 Hz Alternating and Static Magnetic Field from Induction Coil and Permanent Magnets, IEEE Magnetics Letters. 11 (2020), Art no. 2104704. doi:10.1109/LMAG.2020.3021364, Scopus – Q3.

[dis2] **M. Milgrāvis**, A. Bojarevičs, A. Gaile, V. Geža, Application of AC and DC magnetic field for surface wave excitation to enhance mass transfer, Journal of Crystal Growth. 534 (2020), 0022-0248. doi:10.1016/j.jcrysgro.2019.125409, Scopus – Q2.

Publications about particle mixing into the melt by using EM methods:

[dis3] T. Beinerts, A. Bojarevičs, R. Baranovskis, **M. Milgrāvis**, I. Kaldre, Permanent magnet dipole stirrer for aluminium furnaces, IOP Conference Series: Materials Science and Engineering, 424 (2018), 1757-899X. doi:10.1088/1757-899X/424/1/012037.

[dis4] **M. Milgrāvis**, G. Kroņkalns, R. Nikoluškins, T. Beinerts, M. Kalvāns, A. Bojarevičs, I.A. Perianu, Electromagnetic Methods for Production of Aluminium Metal Matrix Composites, Solid State Phenomena. Trans Tech Publications, Ltd. 332 (2022). doi:10.4028/p-9shcqm, Scopus - Q3.

Publications about particle dispersion into the melt by using EM methods:

[dis5] Kaldre, A. Bojarevčs, I. Grants, T. Beinerts, M. Kalvāns, **M. Milgrāvis**, G. Gerbeth, Nanoparticle dispersion in liquid metals by electromagnetically induced acoustic cavitation. Acta Materialia. 118 (2016), 253-259. doi:10.1016/j.actamat.2016.07.045. Scopus – Q1.

[dis6] **M. Milgrāvis**, I. Krastiņš, I. Kaldre, M. Kalvāns, A. Bojarevičs, T. Beinerts, Pulsed and Static Magnetic Field Influence on Metallic Alloys during Solidification. Crystals. 13(2):259 (2023). doi:10.3390/cryst13020259. Scopus – Q2.

[dis7] I. Kaldre, A. Bojarevičs, **M. Milgrāvis**, T. Beinerts, M. Kalvāns, Directional Solidification of Aluminum A360 under Moderate DC Magnetic Field and Electric Current. Materials Research. 26(Mat. Res., 2023 26) (2023). doi:10.1590/1980-5373-MR-2022-0330. Scopus – Q2.

Scientific publications not included in this dissertation

1. R. Baranovskis, D. Berenis, I. Grants, A. Bojarevics, T. Beinerts, **M. Milgravis**, Contactless Aluminum Degassing System—GaInSn Model Experiments and Numerical Study, Journal of Sustainable Metallurgy. 7 (2021). doi:10.1007/s40831-021-00459-8.
2. I. Kaldre, **M. Milgrāvis**, A. Bojarevičs, T. Beinerts, Electromagnetic Processing during Directional Solidification of Particle Strengthened Aluminum Alloys for Additive Manufacturing. Materials Proceedings. 3(1):19 (2021). doi:10.3390/IEC2M-09255.
3. V. Geža, A. Gaile, A. Bojarevičs, **M. Milgrāvis**, Ģ. Zāģeris, S. Pavlovs, Electromagnetically Generated Waves on Free Surface of Liquid Metal for Refinement Process. Conference proceedings: HES - 19 - Heating by Electromagnetic Sources. (2019).

4. I. Kaldre, A. Bojarevičs, T. Beinerts, R. Baranovskis, R. Nikoluškins, **M. Milgrāvis**, M. Kalvāns, Contactless electromagnetic method for aluminium degassing. IOP Conference Series: Materials Science and Engineering. (2018), ISSN 1757-899X. doi:10.1088/1757-899X/424/1/012057.
5. A. Bojarevičs, I. Kaldre, **M. Milgrāvis**, T. Beinerts, Direct chill casting of aluminium alloys under electromagnetic interaction by permanent magnet assembly. IOP Conference Series: Materials Science and Engineering. 355 (2018). doi:10.1088/1757-899X/355/1/012011.
6. O. Budenkova, **M. Milgrāvis**, C. Garnier, A. Gagnoud, Y. Delannoy, S. Semenov, J. Etay, Application of modulated calorimetry to the liquid metals using electromagnetic levitation and static magnetic field. IOP Conference Series: Materials Science and Engineering. 424 (2018). doi:10.1088/1757-899X/424/1/012004.
7. **M. Milgrāvis**, I.A. Perianu, A.C. Murariu, A.V. Bîrdeanu, Adhesion Strength Test Comparison for HVOF Nickel-Based Superalloy Powders on Steel Substrates and Layer Characterization. Advanced Materials Research. 1146 (2018). doi:10.4028/www.scientific.net/amr.1146.126.
8. A. Bojarevičs, R. Baranovskis, I. Kaldre, **M. Milgravis**, T. Beinerts, Two cylinder permanent magnet stirrer for liquid metal. IOP Conference Series: Materials Science and Engineering. Germany: IOP Publishing Ltd. 228 (2017), 1757-899X. doi:10.1088/1757-899X/228/1/012022.

Participation in conferences

The author has presented the obtained results in local and international conferences:

[conf1] **M. Milgrāvis**, G. Kroņkalns, R. Nikoluškins, T. Beinerts, M. Kalvāns, A. Bojarevičs, I.A. Perianu, Electromagnetic methods for production of aluminium metal matrix composites. Innovative Technologies for Joining Advanced Materials, TIMA-21. (2021) Online.

[conf2] **M. Milgrāvis**, T. Beinerts, A. Bojarevičs, I. Kaldre, M. Kalvāns, I. Krastiņš, Electromagnetic methods for production of aluminium metal matrix composites. LightMat 2021. (2021) Online.

[conf3] **M. Milgrāvis**, I. Krastiņš, A. Bojarevičs, Līdzstrāvas un ārējā magnētiskā lauka radīta plūsma uz šķidra metāla virsmas cilindriskā traukā, LU 79. starptautiskā zinātniskā konference. (2020) Online.

[conf4] **M. Milgrāvis**, A. Bojarevičs, V. Geža, A. Gaile, Experiments on Surface Wave Excitation by Electromagnetic Field, International Conference on Crystal Growth and Epitaxy, ICCGE-19. (2019) Keystone, Colorado, USA.

[conf5] **M. Milgrāvis**, A. Bojarevičs, T. Beinerts, R. Baranovskis, Electromagnetic method for Aluminium degassing, LightMat 2019. (2019) Mancheter, UK.

[conf6] T. Beinerts, A. Bojarevičs, R. Baranovskis, **M. Milgrāvis**, I. Kaldre, Permanent magnet dipole stirrer for aluminium furnaces, The 9th International Symposium on Electromagnetic Processing of Materials (EPM2018). (2019) Awaji Island, Hyogo, Japan. The presentation got the best presentation award in conference.

Participation in scientific projects

The development of the doctoral thesis took place within the framework of the following projects. Thank you for funding the research!

1. "Strengthening of the capacity of doctoral studies at the University of Latvia within the framework of the new doctoral model", University of Latvia, identification No. 8.2.2.0/20/I/006. 2021-2022.
2. ERDF project "Electromagnetic technology with nano-particle reinforced light alloy crystallization process for 3D additive manufacturing applications"., University of Latvia, No. 1.1.1.1/19/A/080. 2020-2022.
3. ERAF project: "Refinement of metallurgical grade silicon using smart refinement technologies", University of Latvia, No.1.1.1.1/16/A/097. 2018-2020.
4. Financial support from German Helmholtz Association in frame of the Helmholtz Alliance Liquid Metal Technologies (LIMTECH) project (No. HA-315), University of Latvia, 2014-2017.

NATIONAL DEVELOPMENT PLAN 2020

EUROPEAN UNION
European Social Fund

INVESTING IN YOUR FUTURE

Author's contribution

As part of the doctoral thesis, the author was involved in all research activities including design processes and realization of the experiments, processing of results and other work stages of the described experiments.

While conducting research on surface waves, the author independently developed numerical models for the optimization of the inductor and permanent magnet system [dis1], performed analytical evaluations for the development of a silicon melting chamber and the scaling of EM treatment and its adaptation to

work with silicon. The author was the main person in the implementation of all experiments, processing the results and drawing conclusions. The main results are described in [dis2]. The author is the first author of both mentioned publications. The author supervised a bachelor's thesis on this topic for student Antra Gaile (mark “excellent”), this work received the first K. Erglis memorial scholarship.

The author has been studying the applications of EM methods for production of MMC since 2015. The author participated in the development and assembly of all experimental systems, as well as performed or participated in the implementation of all experiments. The mentioned publications show only a part of the whole volume of experiments conducted within this topic. The author was the main author of the publications [dis3], [dis4] and [dis6], and was involved in the writing of publication [dis5] and [dis7].

Content of the thesis

Structure of this summary

The thesis consists of research described in five publications. The research is presented by dividing the work into three subfields. Accordingly, this summary is divided into three main chapters – surface waves for silicon purification (chapter 1), mixing of particles in metal (chapter 2), dispersion of particle agglomerates in metal (chapter 3).

At the beginning of **Chapter 1**, the motivation of the study and the research so far in surface wave topic are described. The chapter continues with development of the experimental system. The obtained results with surface waves on the melt are presented with various system parameters. At the end of the chapter, the main conclusions are described and the further development of the research by adapting the EM method to work with liquid silicon is shown.

Chapter 2 shows the study of particle mixing into the melt. The chapter begins with overview of the MMC topic and currently used MMC production methods. The chapter continues with description of development of permanent magnet stirrer technology up to an industrial prototype and how the stirring technology was adapted for mixing of particles into liquid metal.

Chapter 3 describes the study of particle dispersion in MMC. The chapter begins with a literature review to show the current research in this topic, as well as presents the conducted experiment and the main results from study with combined B_{AC} and B_{DC} interaction. The chapter continues with the study of pulsed magnetic field interaction for MMC production. At the end of the chapter, the results of the developed continuous casting crystallizer with EM interaction is described, as well as the conclusions and further development of the research.

At the end of this summary, the main conclusions are presented. After the conclusions, acknowledgement and list of references is provided.

Novelty of the study

The experimental system for surface wave experiments is designed specifically for this study. The system consists of a newly designed inductor based on the Bitter coil concept [38] and a new ring-shaped permanent magnet system based on the Halbach assembly [39]. The parameters reached by the EM system are unique and have not been found in the literature. Surface waves generated by alternating magnetic field have been studied in France, SIMAP laboratory [9,10]. In this thesis, the novelty is to use a combination of magnetic fields, which allowed to reach unexplored regimes of wave excitation.

Researchers from University of Latvia Institute of Physics (IP UL) are among pioneers in the development of permanent magnet stirrer technology for metallurgy [26,40–42]. Research of particle mixing into the melt is a continuation of the stirring technology applications. The only possible developer of similar permanent magnet technologies could be the company Zmag Ltd, which develops permanent magnet channel-type stirrers. Researchers have developed an EM method for stirring particles into the melt with an inductor system [24,25], which serves as a direct alternative to the a mechanical rotor in the metal stir-casting process. This technology is in early stage development and is not used in industry yet. Other studies with similar EM technologies for MMC production have not been found in the literature. The use of permanent magnet stirrers for MMC production is considered to be a novelty.

The concept of using combination of alternating (B_{AC}) and static (B_{DC}) m.f. for dispersion of particle agglomerates in metal was initiated by research on ODS steel [43]. The use of EM methods for particle dispersion in aluminum matrix composites is a new sub-field that was started by researchers at IP UL and the author is one of them. There are only few studies about excitation of cavitation by an EM field in liquid metals [7,30,44], so the cavitation generation in specific aluminum and tin alloys and the determination of the physical parameters themselves for the initiation of the effect is considered to be a novelty [30,43,45,46].

The use of pulsed magnetic field for particle distribution in metal matrix composites has so far been studied only in cases where particles are synthesized in melt. Metallurgical applications of combined pulsed and static magnetic field exposure is found in only one study [6], studying the impact of EM exposure on the microstructure of the alloy. In this work, both the developed pulsed interaction and its application are considered to be a novelty that has not been discussed in the literature so far.

Methodology

Since liquid metal is not transparent and the melting point is often relatively high, the number of experimental methods to characterize the processes in the metal is limited. Table 1 shows the properties of the used liquid metals. Liquid silicon has properties similar to metals. During EM method development stages various numerical and physical models have been used. Analytical and numerical models were developed by using Wolfram Mathematica, Mathcad and Comsol Multiphysics and other software. These models allowed to evaluate electromagnetic system parameters, induced force, pressure and flow in liquid metal. Based on the calculations, physical models were built for Galinstan, which is a liquid metal at room temperature. Physical model helped to analyze physical processes in liquids in a **much simpler, more detailed, and safer way**. Galinstan's models have been used in research on surface waves and permanent magnet stirrers for particle mixing into the melt.

Table 1 Liquid metal properties

Parameter	Symbol	Galinstan (liquid)	Silicon (liquid)	Aluminium (liquid)	Tin (liquid)
Melting temp., °C	T_m	~10	1410	660	232
Density, Kg/m^3	ρ	6360	2570	2360	6974
El. conductivity, S/m	σ	$3.3 \cdot 10^6$	$1.2 \cdot 10^6$	$4.1 \cdot 10^6$	$2.0 \cdot 10^6$
Surface tension, N/m	γ	0.3-0.7	0.75	1.0	0.6

To analyze the processes in the melt, Pulsed Ultrasound Doppler Velocimetry (PUDV), photography and filming of the metal surface, including usage of high-speed cameras up to 1000 fps techniques were used. Optical distance measurement with a laser sensor was used to measure surface deformations.

Analytical and numerical models were improved according to the experimental results. EM methods were adapted to the practical applications for silicon and aluminum using dimensionless criteria. Dimensionless criteria allow to adapt the magnetic hydrodynamic (MHD) systems for other metals and scale them. MHD interaction parameter N, dimensionless frequency Ω_d, Hartmann number Ha, Reynolds number Re are the main dimensionless criteria for these

studies. In case of dispersion of particle agglomerates, instead of physical modeling, the sound signal was measured directly from the liquid tin and aluminium during the experiment, allowing to follow the cavitation signal intensity. In the case of PMF, the melt surface deformation was analyzed and compared with the numerical model, which allows to estimate the induced force and pressure.

Optical microscopes, X-ray fluorescence microscopy (XRF) and scanning electron microscope (SEM) were used to analyze the samples after the experiments. Tensile strength of aluminium samples obtained by continuous casting crystallizer were tested according to ASTM E8 standard [47].

1 Electromagnetic excitation of surface waves

1.1 Motivation and proposed concept

The total capacity of installed solar panels in the world has increased 30 times in ten years from 2009-2019 [48]! Silicon is one of the raw materials used in solar panels and directly affects their price. Traditionally, silicon for the semiconductor industry is produced by Siemens process (obtaining EG-Si, mass fraction of impurities 10^{-9}–10^{-11}). The same silicon is also used to produce solar panels, where such pure silicon is not needed. The alternative is to produce solar-grade silicon (SoG-Si, impurity 10^{-6}) through the metallurgical route, which is cheaper. Through metallurgical route most of the metallic impurities with a low segregation coefficient in silicon are removed by directional solidification. The exception is phosphorus and boron impurities which need different purification processes [49,50].

Purification of phosphorus and boron is carried out through the liquid silicon surface. The phosphorus is removed by vacuuming liquid silicon, while boron is removed by blowing argon gas with water vapor (Ar+3% H_2O) onto the silicon surface. Boron concentration in silicon during the purification process can be described by equation (1), where $C_{B,0}$ is the initial boron concentration, $C_{B,t}$ – boron concentration after time t, A – surface area, V – volume, t – time. The coefficient kB is determined experimentally and depends on oxidizing gas type, supply rate and melt temperature.

$$ln\left[\frac{C_{B,0}}{C_{B,t}}\right] = k_b \frac{A}{V} t \tag{1}$$

The motivation of this study is to improve boron removal from silicon by increasing the silicon surface area A with EM-excited surface waves. The silicon temperature required for boron removal is above 1500 °C [50]. At such temperatures mechanical wave excitation would be technically difficult. Electromagnetic excitation of surface waves could be advantageous because waves would be generated in a contactless manner, and there would be no other potential sources of contamination in contact with the liquid silicon.

The development of this EM method can be divided into the following stages:

1) Development of analytical and numerical models.

2) Development of physical model and conduction of experiments with Galinstan.

3) Adaptation of EM method to silicon and development of laboratory prototype.

1.2 Theoretical background

The equations of electromagnetism and flow dynamics can be used to describe the flows that occur in a liquid metal when a magnetic field is present. In general, electromagnetism in the following systems is described by Maxwell's equations (2-5):

$$\nabla \cdot \vec{E} = \frac{\rho_q}{\varepsilon_0} \tag{2}$$

$$\nabla \cdot \vec{B} = 0 \tag{3}$$

$$\nabla \times \vec{\mathrm{E}} = -\frac{\partial \vec{B}}{\partial t} \tag{4}$$

$$\nabla \times \vec{\mathrm{B}} = \mu_0 \left(\vec{J} + \varepsilon_0 \frac{\partial \vec{E}}{\partial t} \right) \tag{5}$$

In the equations $\vec{E}$ – electric field, $\vec{B}$ – magnetic field induction, $\vec{J}$ – current density, ρ_q – charge density, μ_0 – vacuum magnetic permeability, ε_0 – electric constant, t – time.

In an electrically conductive medium, currents are induced according to Faraday's law of induction (4). The Lorentz force (6) acts on a moving, charged particle and consists of the particle's interaction with the electric and magnetic fields. In the equation q – charge, $\vec{u}$ – velocity.

$$\vec{f} = q(\vec{E} + \vec{u} \times \vec{B}) \tag{6}$$

In a continuous medium, it is more convenient to use not the Lorentz force per individual particle, but the force per unit volume. The expression of the Lorentz force can be transformed into (7) – the individual charge can be replaced by the charge density q_e and the product of the charge density and the area velocity by the current density $\vec{j} = \rho_e \vec{u}$, where ρ_e – the full charge density, σ – electrical conductivity. Current density is obtained from Ohm's law (8).

$$\vec{f} = \rho_e \vec{E} + \vec{J} \times \vec{B} \tag{7}$$

$$\vec{J} = \sigma(\vec{E} + \vec{u} \times \vec{B}) \tag{8}$$

It can be assumed that the electric field $\vec{E}$ in volume tends to zero [10,51], accordingly, only the second term dominates in the Lorentz force expression. As a result, equation (7) reduces to (9):

$$\vec{f} = \vec{J} \times \vec{B} \tag{9}$$

From the law of charge conservation follows the current continuity equation (10). Since ρ_e is small, the right side of the equation tends to 0.

$$\nabla \cdot \vec{J} = \frac{\partial \rho_e}{\partial t} \tag{10}$$

In Ampere's law, displacement current $\varepsilon_0 \frac{\partial B}{\partial t}$ can be neglected, accordingly this equation also simplifies. By summarizing the assumptions made, a system of equations (11) is created. This system can be used to describe electromagnetism in the research presented below [51].

$$\begin{cases} \nabla \times \vec{B} = \mu_0 \vec{J} \\ \nabla \cdot \vec{J} = 0 \\ \nabla \times \vec{E} = -\dfrac{\partial \vec{B}}{\partial t} \\ \nabla \cdot \vec{B} = 0 \\ \vec{J} = \sigma(\vec{E} + \vec{u} \times \vec{B}) \\ \vec{F} = \vec{J} \times \vec{B} \end{cases} \tag{11}$$

By combining Ohm's, Faraday's, and Ampere's laws, the magnetic field transport equation (12) is obtained. It describes changes in the magnetic field over time. On the right-hand side of the equation, the first part is responsible for the advection of the magnetic field or how the flow of an electrically conductive liquid with velocity u transfers the magnetic field. The second part describes the m.f. diffusion, where $1/\sigma\mu$ is the diffusion coefficient.

$$\frac{\partial \vec{B}}{\partial t} = \nabla \times \left(\vec{u} \times \vec{B}\right) + \frac{1}{\sigma\mu} \nabla^2 \vec{B} \tag{12}$$

The dynamics of an incompressible fluid flow can be described by the Navier-Stokes equation (13), where the left-hand side of the equation is the convective derivative of the flow velocity, while the first term on the right-hand

side is the pressure gradient. The second term describes the velocity field diffusion, the third term describes the gravitational force, and the fourth term describes the Lorentz force. In the equation ρ – density, η – dynamic viscosity, $\vec{g}$ – gravitational constant.

$$\rho\left(\frac{\partial\vec{u}}{\partial t}+\vec{u}\cdot\nabla\vec{u}\right)=-\nabla p+\eta\nabla^2\vec{u}+\rho\vec{g}+\vec{J}\times\vec{B} \tag{13}$$

For physical modeling of surface waves Galinstan is used. In the following description it is assumed that the metal is in a cylindrical crucible and an axially symmetric magnetic field is applied. It is chosen to use 50 Hz current for magnetic field generation, so the EM method is more effective in potential industrial applications. The properties of liquid silicon and Galinstan alloy are shown in Table 1. Dimensionless parameters are used to compare and predict physical processes in both melts. One of the main parameters for such system description is the MHD interaction parameter N (14), which characterizes the ratio of electromagnetic and inertial forces.

$$N=\frac{\sigma}{\rho}\frac{B^2}{\omega} \tag{14}$$

In case of silicon and Galinstan, N is almost the same, since both fluids have similar ratios of electrical conductivity σ and density ρ. In the equation, ω is the cyclic frequency.

Another important dimensionless parameter is the dimensionless frequency Ω_d (15), which describes how strong skin-effect $\delta=\sqrt{\frac{2}{\mu_0\mu\sigma\omega}}$ affects the system. In equation (15) R is system radius and μ_0 is the magnetic constant.

$$\Omega_d=\sigma\omega\mu_0R^2 \tag{15}$$

Hartman number and ratio of magnetic fields B_{DC}/B_{AC} are also important parameters for description of the system.

It is known that gravitational waves on the surface of liquid can be generated by time averaging force. For short waves $h\cdot k>>1$ equation (16) can be used, where h – depth of the liquid, k – wave number, g – gravitation constant and γ - surface tension [52].

$$\omega^2=gk+\frac{\gamma k^3}{\rho} \tag{16}$$

During experiments Galinstan surface is covered with oxide layer and surface tension can vary in a wide range from 0.3 to 0.7 N/m, so the wavelength $\lambda = \frac{2\pi}{k}$ varies in range of 5 to 7 mm.

Electromagnetically generated surface waves were studied theoretically and experimentally by J.M. Galpin, I. Fautrelle and A.D. Sneyd [9–11]. This study showed that the generated waves are axisymmetric standing waves with a frequency of 2f, if the frequency of the alternating magnetic field is f. The study also discussed the importance of viscosity and surface tension. By studying the effect of B_{AC} on liquid mercury in the low frequency range (2 – 20 Hz), it is experimentally shown that the dominant force in the system changes depending on the dimensionless frequency. Due to the skin effect, two cases can be distinguished, firstly, if the dimensionless frequency $\Omega_d \leq 1$, the time-average force is minor compared to the force amplitude, secondly, if $\Omega_d > 1$, the time-average force becomes dominantly large, without forming surface waves [9,10]. By using a constant temperature flow meter, Galpin and Fautrell had measured the flow of metal in mercury experiments, thus characterizing the average flow velocity and turbulence in the crucible. During the experiments on the surface of mercury standing waves were observed. The wave structure can be divided into two categories - concentric and azimuthal. The induced wave patterns were divided into four regimes: (I) axisymmetric standing waves with the dominant frequency 2f, (II) axisymmetric standing waves and azimuthal waves, (III) concentric waves are replaced by large-amplitude azimuthal waves, (IV) chaotic deformations of the free surface.

In metallurgical processes surface deformations are often undesirable, as they can promote, for example, metal oxidation. For practical applications mechanisms to suppress or stabilize the metal flow and resulting surface deformations are widely studied. The use of a static magnetic field is proposed in the literature as a solution [12,13,53]. The mentioned studies studied surface deformations induced by EM field and mechanical vibrations. If the surface deformation is caused by an electromagnetic field, then the static magnetic field affects the system in two ways - firstly, it interacts with the currents in the metal and generates a Lorentz force, and secondly, it damps the flow of liquid metal. Studies mostly discuss the flow damping effect, while in this work the focus is to use B_{DC} to generate surface waves over the entire metal surface.

The electromagnetic force on the side surface of an axially symmetric area of liquid metal according to the solution by Juris Krumins [54] is shown in Figure 1.

To generate surface waves in case when the dimensionless frequency is greater than 1, this study proposes to use a combination of B_{AC} and B_{DC} magnetic fields. In that case, the force density (17) induced in the melt consists of two parts – the induced current $\vec{j}$ interaction with alternating m.f. and static m.f.

$$\vec{f} = \vec{j} \times (\vec{B}_{AC} + \vec{B}_{DC}) \tag{17}$$

If $\vec{B}_{AC} \ll \vec{B}_{DC}$, the dominant is the product of induced current and B_{DC}, so the forcing frequency matches with B_{AC} frequency, but the force amplitude is significantly higher, see Figure 1 on the right.

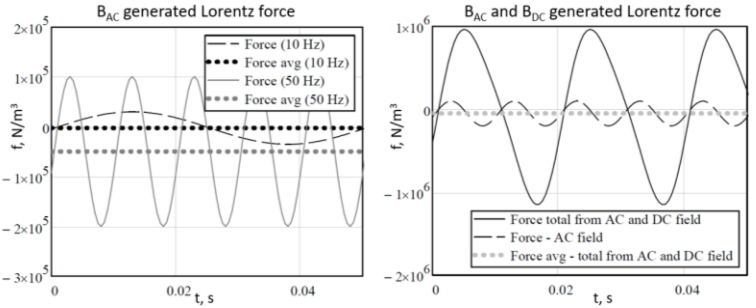

Figure 1 The induced force at the wall of an axially symmetric liquid metal region. Left - time-varying and time-average force at 10 Hz and 50 Hz. On the right - force amplitude with and without static magnetic field

Without considering viscous and capillary forces, the flow rate U in the crucible can be estimated using the Navier-Stokes equation (18).

$$\rho\vec{U}\omega + \rho\frac{\vec{U}^2}{\delta} = \sigma(\omega\delta\vec{B}_{AC} - \vec{U}\vec{B}_{DC})(\vec{B}_{AC} + \vec{B}_{DC}) \tag{18}$$

The right side of equation (6) describes the electromagnetic forces. In the first brackets, the first part is responsible for the induced current that generates the flow, while the second part describes the damping effect that occurs when melt flows in a magnetic field. If the dimensionless frequency of the system $\Omega_d \geq 1$, the skin depth thickness δ should be used instead of the crucible radius R.

Figure 2 shows the flow rate U as a function of static magnetic field. The maximum flow rate is at $B_{DC} \approx 0.4$ T. If B_{DC} continues to increase, the damping effects begin to dominate and the velocity decreases.

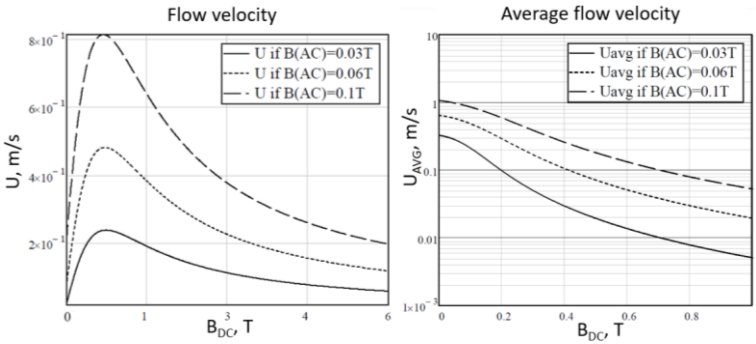

Figure 2 Combined alternating and static magnetic field velocity.

B_{DC}≈0.4 T is chosen as a static magnetic field value for the experimental system. Two crucible diameters are chosen to conform the system with $\Omega_d > 1$ and $\Omega_d < 1$.

1.3 Experimental system

For experimental system, the following criteria were set:

1) The system must provide a crucible dimensions of which correspond to the situation where $\Omega_d < 1$ and $\Omega_d > 1$. $\Omega_{d,max} = 4$.
2) B_{DC}≈0.4 T at the center of the system.
3) To estimate the wave intensity limits, the maximum BAC amplitude should reach B_{AC}≈0.3 T.
4) The space above the crucible must be free to obtain photo and video materials.

A sketch of the experimental setup is shown in Figure 3 - the crucible is surrounded by an inductor as a B_{AC} source and a permanent magnet system as a B_{DC} source. At the center of the system B_{DC} direction is perpendicular to the melt surface (parallel to the B_{AC}).

The inductor consists of 60 rings, which are sequentially connected with electrical contact, forming an electrical circuit in the form of a spiral as in a Bitter inductor [38]. The inductor consists of 56 electrical windings, which are water cooled from the outer surface. Inductor provides B_{AC} up to 0.33 T. The B_{DC} field source is an axially symmetric permanent magnet system based on the Halbach magnet assembly principle [39]. The magnetization direction of the magnet blocks is shown in Figure 3, the magnetic field lines are illustrated by black dashed lines.

The magnet system consists of 192 Nd-Fe-B permanent magnets surrounded by a ferromagnetic yoke. B_{DC} magnetic field in the center is B_{DC}=428

mT. The created inductor, magnet system and the experimental system itself are shown in

Figure 4.

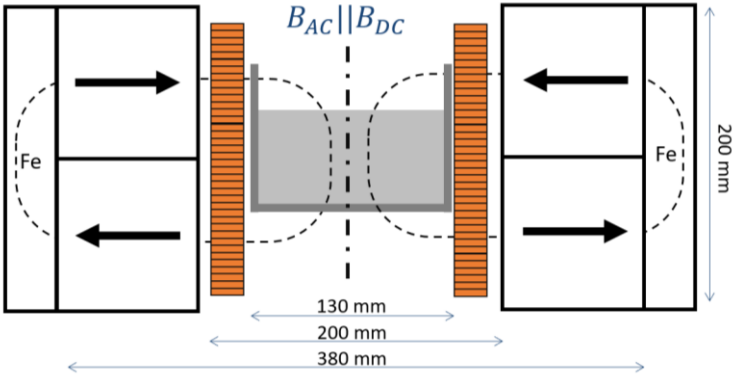

Figure 3 Schematic drawing of experimental system for the excitation of surface waves in Galinstan. The orange rectangles illustrate the created Bitter inductor. The direction of magnetization of the permanent magnets is represented by the black arrows; the black dashed line illustrates the magnetic field lines. Both B_{AC} and B_{DC} are perpendicular to the melt surface.

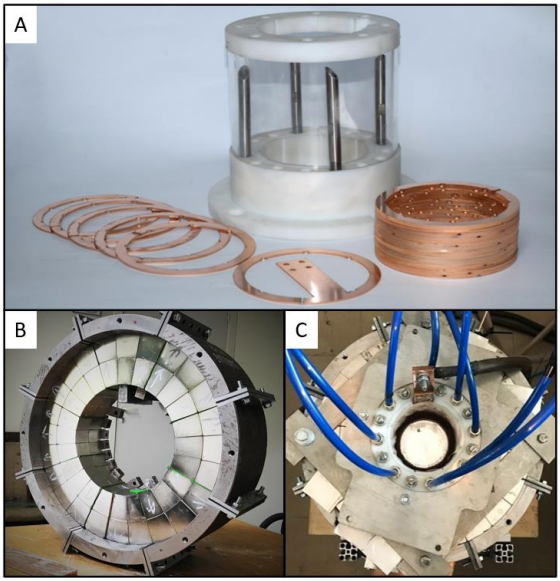

Figure 4 Pictures A and B show the inductor and permanent magnet system during assembling process. Picture C shows the assembled experimental system from above.

More detailed description of the system, including the obtained magnetic field distributions are provided in publication [dis1].

1.4 Experimental results

Two types of EM interactions are experimentally studied:

a) Melt is in an alternating magnetic field (B_{AC}). The field is perpendicular to the melt surface.
b) Melt is in an alternating and static magnetic field (B_{AC}+B_{DC}), both fields are parallel, perpendicular to the melt surface.

Both cases are considered for two crucible sizes:

1) Crucible diameter 52.6 mm, Ω_d=0.94.
2) Crucible diameter 96.7 mm, Ω_d=3.19.

For Ω_d=0.94 in B_{AC} exposure, surface waves were observed over the entire metal surface, see Figure 5 top row. As the field intensity increases, the waves gradually change from concentric (B_{AC}=25 mT) to non-linear (B_{AC}=72 mT). Similarities can be observed with the experiments conducted by Fautrelle [9], where the transition from concentric to nonlinear waves was studied in detail.

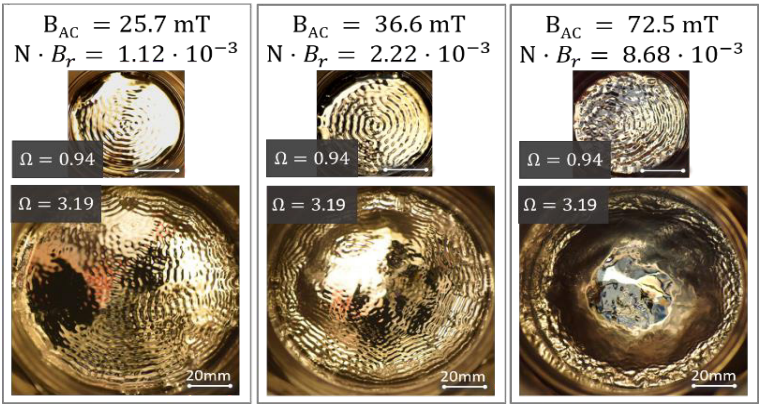

Figure 5 Surface waves depending on the intensity of B_{AC} exposure (50 Hz), for two different crucible sizes.

In case with a larger crucible diameter (Ωd=3.19), the wave formation takes place near the crucible walls. At low intensities (B_{AC}=25 mT), waves can be observed over the entire surface, but the wave amplitude decreases towards

the center. By increasing the B_{AC} intensity above 30 mT, intense turbulent metal flow and meniscus formation in the center of the system can be observed. As the B_{AC} increases, the meniscus becomes larger, while the excited waves are less visible on the surface of the meniscus, see Figure 5 bottom row images. Meniscus height grows from 5 mm at B_{AC}=50 mT reaching 15 mm at B_{AC}=90 mT. Video recording with a 960 fps camera shows that the surface **waves are concentric and are traveling to the center**. During the analysis of the video recordings, it was measured that the speed of the waves is in the range of 70-90 cm/s. The speed depends on the position where the measurement was made.

In a series of experiments with a combined B_{AC} and B_{DC} magnetic field, the wave intensity increases significantly. By starting the experiments with combined exposure at B_{AC}=146 mT, wave intensity was so high that the melt started to splash due to droplets separating from the wave crests. At B_{AC}+ B_{DC} exposure surface waves already formed at B_{AC}=10 mT. The height of the waves at B_{AC}=16 mT and B_{DC}=428 mT is even greater than in all the considered cases with higher intensity, but only B_{AC} exposure, see Figure 6. By using 960 fps camera, it was recorded that up to B_{AC}=12 mT the **waves are concentric and traveling towards the center**. The speed of the waves is within 45-55 cm/s. At both crucible sizes (Ω_d=0.94 un Ω_d=3.19) **meniscus formation was not observed on the metal surface**. The meridional flow along the symmetry axis was negligible in this case and could not be measured with pulsed Doppler ultrasound velocimetry (PUDV).

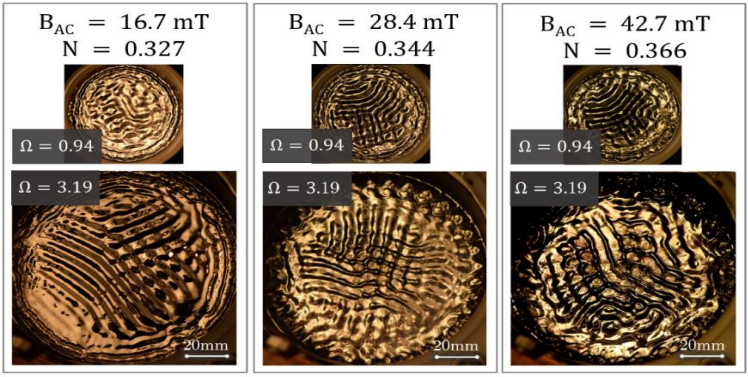

Figure 6 Surface waves depending on B_{AC} intensity in combination with parallel B_{DC} = 428 mT magnetic field.

With a combination of B_{AC} and B_{DC}, waves of similar intensity are obtained as four times the effect of only B_{AC} field. From the used electrical

energy point of view, by using the combined magnetic fields waves can be obtained with approximately ~16 times less electric energy consumption.

The wavelength with only B_{AC} exposure was within the range of 2 to 5 mm, and with $B_{AC} + B_{DC}$ from 5 to 7 mm. The results are described in more detail in the publication [dis2]. Assuming that the surface waves are concentric, and their surface can be described by the analytical expression $y(x) = d \sin \frac{\pi n x}{L}$, the length of the line from the center to the edge can be determined by the formula (19), where d is wave amplitude and n is number of waves.

$$b = \int_0^L \sqrt{1 + \left(\frac{dy}{dx}\right)^2} = \int_0^L \sqrt{1 + \left(\frac{\pi n d}{L} \cos \frac{\pi n d}{L}\right)^2}\, dx \qquad (19)$$

If there are no waves on the surface, the length of line b is the radius of the system $b_0 = L$. The obtained surface area ratio $Q = s/s_0$ can be used to evaluate the increase of surface area for given wavelength and amplitude, see Figure 7. This evaluation does not consider the meniscus if only B_{AC} is applied.

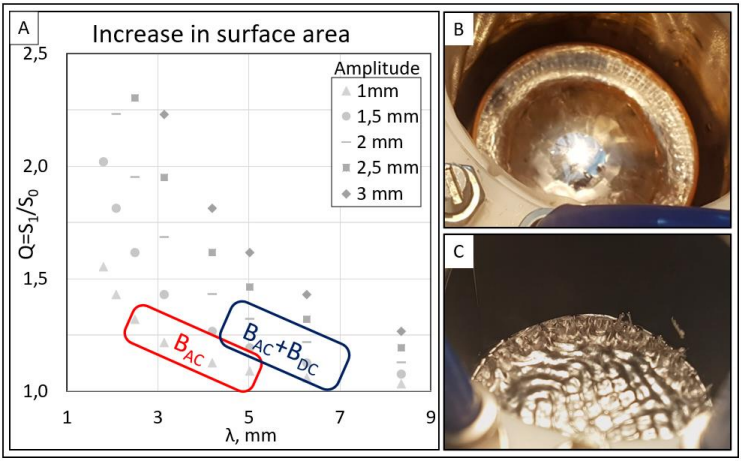

Figure 7 A) Graph shows the increase in surface area for B_{AC} and $B_{AC}+B_{DC}$ exposure with different wave amplitudes. B) Wave excitation limit with only B_{AC} – too intense meniscus formation. C) Wave excitation limit with $B_{AC}+B_{DC}$ - splashes are formed.

The maximum increase in surface area with both types of exposure is limited. In the case of B_{AC} exposure, by B_{AC} increase the waves gradually are less and less observed on the gradually growing meniscus. In case of $B_{AC}+B_{DC}$ around N=0.366, the amplitude of the waves no longer increases, but the splash drops are formed. A potential explanation for these splashes could be the "singing

bowl" effect, which also occurs in the case of mechanically excited surface waves [55]. The amplitude of the waves in experiments with B_{AC} exposure did not exceed 1 mm, but with B_{AC}+B_{DC} did not exceed 2 mm. Accordingly, the maximum surface area increase within the context of the developed method is about 1.3 times.

1.5 Conclusions and further technology development

1.5.1 Conclusions

1. The pictures of surface waves (Figure 5, Figure 6) show that the developed combination of B_{AC} and B_{DC} magnetic fields allows to generate intense surface waves in dimensionless frequency range from 0.5 to 4.
2. 960 fps video recording shows that both B_{AC} and combined B_{AC} and B_{DC} with low B_{AC} intensity produces concentric surface waves which are traveling toward the center.
3. The static magnetic field allows to significantly reduce the required intensity of the B_{AC} field for the excitation of surface waves. With a combined field, waves with similar intensity were obtained with four times lower B_{AC} field value – electric energy consumption is ~16 times lower!
4. The maximum intensity of the surface waves generated by combined B_{AC} and B_{DC} field is limited droplet splashes. The maximum surface increase obtained is ~30%.
5. The formation of an oxide layer on the surface of the liquid metal affects the shape and intensity of the generated surface waves. A thick oxide layer reduces the amplitude of the surface waves, but by increasing the B_{AC} intensity the waves stay concentric for longer.

1.5.2 Further technology development – prototype for silicon

According to the physical model, a laboratory prototype for the silicon purification from boron has been developed. The prototype is equipped with an inductor specifically created for this purpose. Experimental realization of this system is technically difficult, as several criteria must be considered. The system provides:

1. Silicon overheating up to 1600 °C.
2. The necessary gas flow for boron removal – controlled Ar+3wt%H_2O flow on the melt surface.
3. Inductor surrounds the furnace. $B_{AC,max}$=170 mT. Inductor cooling system can remove the Joule heat from the windings and thermal radiation from furnace.
4. System allows to take liquid silicon samples during the experiments.

The system is axially symmetrical and consists of 6 MoSi2 heaters, which are covered by zirconium ceramic thermal insulation, see Figure 8. A quartz tube can be introduced into the silicon chamber from above to extract a sample of liquid silicon.

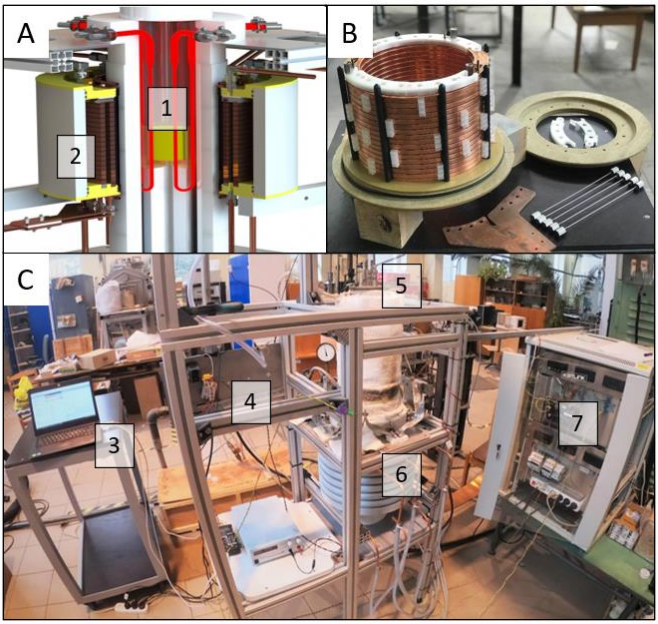

Figure 8 Laboratory prototype for silicon. A) Schematic drawing of the experimental system – 1. furnace chamber with MoSi2 heating elements and a crucible for silicon; 2. inductor with water cooling system; B) Inductor during assembling, the white and black parts are 3D printed. C) Experimental system – 3. temperature and gas flow control; 4. gas heating and humidification; 5. silicon melting furnace; 6. gas introduction and holes to take samples; 7. control of heating elements.

The inductor is made of two copper spirals by making 34 windings in total. The maximum current is 1300 A which corresponds to B_{AC}=170 mT in the center. One of the main challenges during the inductor design process was to remove thermal radiation from the furnace to avoid overheating of the inductor. The water-cooling system allows water flow through the windings with a flow rate >10 L/min. 3D printed parts were used as the coil's construction elements for maximum water flow rate.

The developed electromagnetic technology for surface wave excitation has reached technology readiness level 4 (TRL 4)[14].

2 EM method for particle mixing into the melt

2.1 Motivation and proposed concept

The growing demand for low-cost, high-performance materials has fueled the shift from alloys to composites. Metal matrix composites (MMC) are materials in which non-magnetic particles are mixed into the metal, thus providing significant improvement in thermal or mechanical properties comparing to the base material, such as tensile strength, hardness, wear resistance and crack resistance.

Aluminum and its alloys have attracted wide interest as a base metal to produce aluminum matrix composites (AMC). AMCs are widely used in aviation, automobile, and other industries, where the relationship between the weight of parts and their mechanical properties is important [18,56,57]. Additive manufacturing is considered to be one of the potentially promising applications for AMCs. Figure 9 shows the number of scientific publications in the last 20 years depending on the searched keywords using the Scopus database. The search results show both a significant increase in research related to AMC and additive manufacturing, as well as both topics together. One of the searched keywords is aluminum and silicon carbide (SiC) nano-particles, which is considered to be one of the most promising metal-particle pairs [18,58,59].

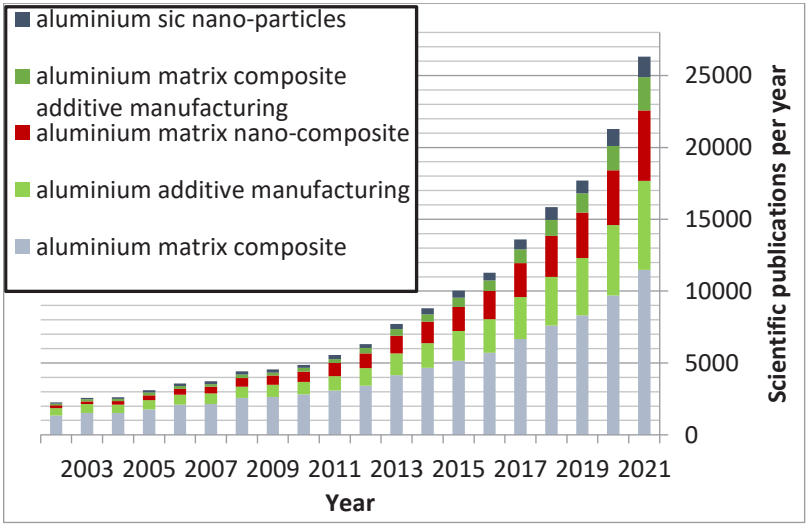

Figure 9 The number of scientific publications in the last 20 years, searching for keywords that describe relevance of the research topic. Data from Scopus database.

AMC production can be divided into two categories - production through the solid phase and through liquid or metallurgical phase of the alloy. The most widely used method through solid phase is powder metallurgy. Although the method is widely used in industry, its main drawback is the need for aluminum powder. Metallurgical AMC production has been in development for 50 years and is much more profitable 4-11 $/kg, comparing to powder metallurgy costs 22-37 $/kg, which are made up mainly due to raw materials themselves [60]. Among the metallurgical production methods, the AMC stir-casting is the most popular. In stir-casting a rotating blade immersed in the alloy is used. The main disadvantage of the stir-casting method is that the mixing is mechanical, which results in blade erosion contaminating the alloy and the alloy tends to stick around the blade. The blade creates intense surface deformations which increase the oxidation of the alloy and results in material losses [18,60,61]. A relatively similar method of particle mixing into the metal is compo-casting in which also rotating blade is used to mix particles into the melt, but the melt is into a semi-solid (slurry) state. The particles mixed into the alloy to produce AMC can be characterized by particle size, chemical composition, shape, addition amount and other parameters. The most effective AMC production method often depends on what particles and alloy are used, as this is determined by the wettability, density and other properties of alloy and particle pair. The AMC production method also depends on the end material application [18,61].

AMC materials can be divided in two parts depending on particle size - micro and nano-sized particles. Properties of the alloy changes significantly depending on the size of the particles and their distribution. For example, Zhao [62] has shown how the tensile strength of the material improves as the SiC particle size decreases by using 10 μm, 1 μm and 50 nm particles and AZ61 aluminum alloy. As the particle size decreases, the particles tend to form agglomeration even more and material is not homogenous. An electromagnetic method for dispersion of particle agglomerates is studied in Chapter 3. A more detailed literature description of AMC production methods is given in [dis4].

Electromagnetic methods for producing AMC alloys by stirring melt with an induction coil have been studied by research groups in India. The method is promising, but it is still at an early stage of development [24,25]. The concept idea is similar to induction stirrers used in metallurgy, for example by ABB [1].

In this thesis a new EM method for particle mixing into the melt is investigated to find an alternative to the stir-casting method by making MMC production more efficient. During the study permanent magnet stirrer technology for industrial size aluminum furnaces [dis3] was developed. Afterwards, the technology was adapted for particle mixing in aluminum alloys. A permanent magnet stirrer in combination with induction heating is used for MMC production [dis4].

This study for development of an EM method for mixing of particles into the melt can be divided into the following stages:

1) Physical model for flow studies in Galinstan melt.

2) Validation of the analytical and numerical models, as well as the technology adaptation for aluminum.

3) Development of an industrial-scale facility for aluminum.

4) Stirring technology adaptation for mixing of particles into the melt, as well as experiments with different particle introduction methods.

2.2 Technology development and adaption for MMC production

2.2.1 Permanent magnet stirrer technology development

In this study the experience gained from cylindrical permanent magnet (PM) stirrers developed in IP UL MHD Technology laboratory is used. The author has been one of the technology developers[26,40,42].

Liquid metal stirring was studied by using Galinstan model, shown in Figure 10 on the left. System consists of container with Galinstan which is as a model for aluminium furnace.

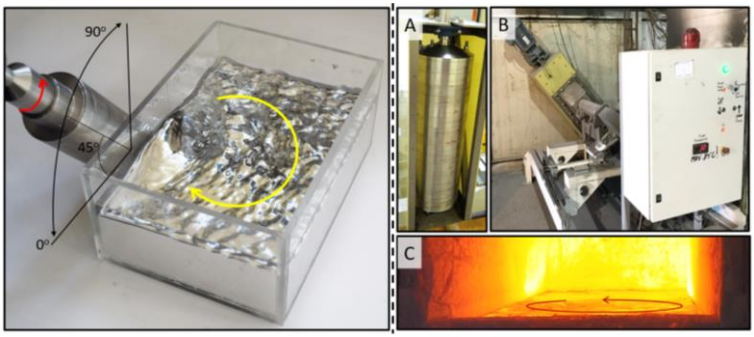

Figure 10 On the left – experimental model with a permanent magnet stirrer for liquid Galinstan (1-1.5 Liters). On the right - scaled permanent magnet stirrer for a 20-ton aluminum furnace (~7,000 Liters). A) Permanent magnet system, B) Stirrer on the furnace wall. The magnet is placed at a 45° angle. C) Intense liquid aluminium flow is observed.

Permanent magnet stirrer is cylindrical shape permanent magnet rotor, which is magnetized radially and rotates along the axis. Stirrer can be set in various angles next to the container wall or under the container. Liquid metal flow distribution generated by a cylindrical permanent magnet rotor (50 mm in diameter, 100 mm in height) was measured by ultrasound Doppler anemometer

(PUDV) for different stirring speeds and metal layer thicknesses. These measurements are used to validate analytical and numerical models for liquid metal flow calculations developed by laboratory colleagues Andris Bojarevičs, Didzis Berenis and Ivars Krastiņš, using open access programs OpenFoam, Elmer etc.

According to the developed numerical models, the technology was developed to an industrial scale – a permanent magnet stirrer was created for a 20-ton aluminum furnace installed in an aluminum factory, see Figure 10. Unlike in channel systems, in aluminum metallurgy the furnace wall thickness can reach 20-30 cm, so classic MHD pumps with multipole rotors cannot be used [63]. These models were also successfully used for research on aluminum degassing technology and scrap mixing into liquid metal [64,65].

The most important result of the research described in the publication [dis3] is the technology transfer to the industrial environment, because in aluminum metallurgy such technology and such large permanent magnet system is used for the first time! These industrial tests show that permanent magnet technologies can be adapted to aluminum metallurgy. The technology is developed up to TRL 7 [14]. As a result of the publication, several aluminum and steel manufacturers (Borbet Austria Gmbh, M.D.Steels, etc.), as well as scientific institutions (Research Institute of Industrial Science & Technology, Korea) have shown interest in this technology.

This research continues with the development of permanent magnet stirrer technology for mixing particles into the aluminum alloys to produce AMC.

2.2.2 Particle mixing into the aluminium alloys

Initially, the idea was to test the concept where the melt is intensively stirred with PM stirrer and particles are spread on the melt surface. With the experimental system it was possible to place a stirrer under or at the side of the crucible, generating an intense flow in the crucible. Initially, particle mixing was tested with A356, A360 and 6061 alloys and different particles – silicon carbide SiC (20 μm), SiC (50 nm) and tungsten carbide WC (50 nm). In all cases, the mixing of particles was unsuccessful because of the oxide layer on the melt surface. Particles tended to stick or remain on oxide layer by forming large agglomerates. Even with intense stirring the oxide layer was not broken and the particles remained on the surface. If the oxide layer was broken, the particles were pushed back to the surface due to poor wettability with alloy.

It has not been observed that particle mixing into the melt would be promoted by any of the methods recommended in the literature:

1) Particle preheating for 2 to 4 h at 700 °C [21,66]
2) Alloy overheating up to 900 °C [67]
3) Provision of an argon atmosphere [60,68]

4) Alloying the melt with 3-5%wt magnesium [69,70]

After the unsuccessful result, a new concept was developed to mix the particles into a semi-solid alloy instead of a liquid. Firstly, the idea came from literature studies on the "compo-casting" method [71], where similarly to “stir-casting” a mechanical rotor stirring is used, but the metal is in a semi-solid state. Secondly, from the neutron radiography experiments carried out by colleagues as part of another research project in which gadolinium particles were stirred into tin – efficient particle mixing from the surface was observed when the alloy was partially frozen [72].

Two concepts for mixing particles in a semi-solid alloy are considered - firstly, the flow is created by a PM stirrer placed at the side of the crucible, and, secondly, the rotor is placed at the bottom, see Figure 11. Flow calculations depending on the position of the magnet are studied by Ilmārs Grants [73].

The alloy is kept hot by the applied high frequency inductor. The inductor allows to maintain the temperature within the necessary temperature range, so the alloy remains semi-solid for a long time. For the A360, A356 and 6061 alloys this range is within 10-20 degrees. The inductor is placed at the bottom of the crucible where alloy is mostly liquid, the semi-solid part is formed at the top of the crucible where the particles are introduced.

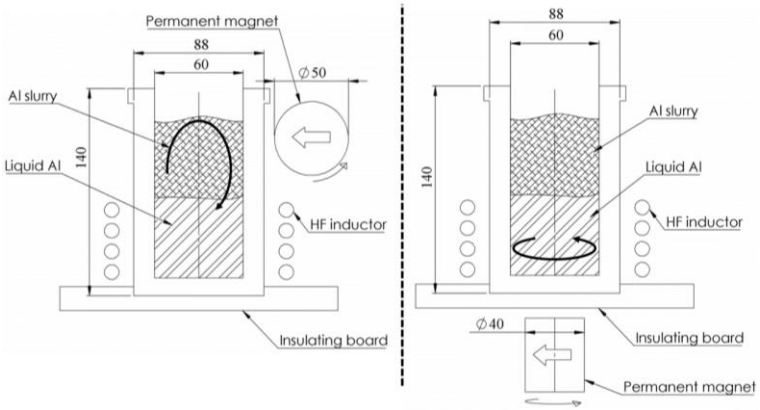

Figure 11 Schematic drawing of experimental setup for mixing particles into a semi-solid alloy. On the left – stirrer is one the crucible side; On the right – stirrer is under the crucible.

2.3 Results of the particle mixing into the melt

With all experimented alloys - A356, A360 and 6061 - it was possible to find a stationary state when the metal remains semi-solid for a long time. A

temperature gradient of ~20 °C between the top and bottom of the crucible was measured with a thermocouple. With both stirring configurations, effective stirring was visually observed, see Figure 12. The flow of metal stopped just a moment before completely freezing.

Figure 12 Stirring of a semi-solid (~610 °C) A360 alloy - intense surface deformations caused by a PM stirrer on the side of the crucible (left), vortex flow caused by a PM stirrer below the crucible (right).

Four methods for particle introduction into the melt have been experimentally tested, see Figure 13:

1) Particles are wrapped in aluminium foil and introduced into the melt. The process is carried out in argon atmosphere.

2) Particle loaded aluminum tubes are introduced into the melt. Tubes are created under argon and pre-heated before introducing them into the melt.

3) Tablets are created from particle and aluminum powder by using a 5t hydraulic press. Tablets are formed from aluminum and SiC (20 μm) powder in argon atmosphere and pre-heated to 350 °C.

4) Particles are poured on the melt surface. Particle pre-heating and argon atmosphere were provided during the experiments.

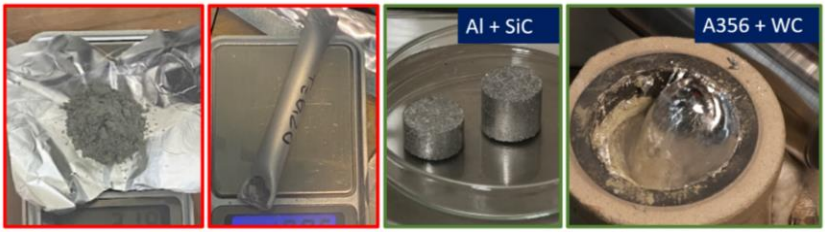

Figure 13 Experimentally tested methods for particle introduction. From the left – particles loaded foil, particle loaded tube, tablets of particle and aluminum powder, particles poured on the melt surface.

From all the mentioned particle introduction methods, during the experiments the third and fourth could completely or partially mix the particles into the metal volume. Sample analyzes with XRF show increase in tungsten and silicon concentrations after particle introduction, see Table 2.

Table 2 XRF sample analysis – increased concentration of SiC and WC is represented by arrows in the table.

Alloy	Particles	Particles, wt%	XRF: WC	XRF: Si	Stirring
6061 ref	-	0%	0	**0,65 %**	
6061	SiC (20µm)	1%	0	**1,09 %**	From bottom
A360 ref	-	0%	**0**	**8,01 %**	
A360	SiC (20µm)	2%	0	**9,56 %**	From bottom
A360	WC (50nm)	1%	**0,23 %**	7,99 %	From side
A360	WC (50nm)	2%	**0,75 %**	8,04 %	From side

WC (50 nm) particles were mixed into the A360 alloy by spreading them on the melt surface, the stirring was carried out from side. The particles were stirred into the melt for about 10-15 minutes and after repeated melting of the alloy, particles did not appear on the surface.

During experiments, it was possible to stir SiC (20 µm) particles into the alloy in the form of tablets by setting the stirrer under the crucible. Using the configuration where the magnet was under the crucible, it was possible to achieve a magnet rotation frequency of up to 400 Hz. Such stirring created melt flow of up to 10 cm/second. During the particle introduction, the tablets had to be mechanically pressed under the surface in an area with intense flow. The tablets in the metal gradually broke. The particles were not pushed out of the metal volume even after remelting.

2.4 Conclusions and further technology development

2.4.1 Conclusions

1. The developed prototype for a 20-ton aluminum furnace (Figure 10) has shown that permanent magnet systems can be scaled and effectively applied in aluminum metallurgy.
2. Permanent magnet stirrer can create intense flow in a semi-solid alloy and break the melt oxide layer until the metal completely freezes (Figure 12).

3. XRF measurements confirm the creation of AMC - SiC particles into the 6061 alloy and the WC and SiC particles into the A360 alloy – by using a combination of induction heating and a permanent magnet stirrer. The process is affected by particle and alloy pair, stirring pattern and particle introduction method.

2.4.2 Further technology development – detailed production methodology

The obtained results qualitatively show that particles can be mixed into the melt with performed EM method. For further technology development, it is planned to quantify these results by determining the necessary stirring parameters, stirring duration, the maximum mass fraction of particles, and to develop detailed methodology for specific alloy and particle pairs. It is essential to develop this methodology also for larger melt volumes.

3 Dispersion of particle agglomerates in the melt

3.1 Literature review

The motivation of the research described in this chapter is similar to the one described at the beginning of Chapter 2, because both studies are focused on EM methods to produce MMC materials, although for different production steps.

When particles are mixed into the liquid metal, they tend to form agglomerates due to surface tension and Van der Waals forces [17]. For micro-sized particles, techniques to disperse particle agglomerates are studied, while for smaller particles with a typical size of <1 μm, the particle homogeneous dispersion in the metal volume is still an unsolved problem. For aluminum and other low melting temperature alloys dispersion of particles can be achieved by mechanical sound generation using sonotrode [74,75]. With an ultrasonic probe (sonotrode), intense pressure oscillations are generated in the melt. Pressure oscillations can cause cavitation in the liquid. The biggest drawback of the mechanical ultrasound generation is the efficiency, since the cavitation zone is only near the probe.

Electromagnetically induced intense pressure oscillations are considered to be one of the contactless alternatives for cavitation generation [76,77]. As a result of pressure oscillations gas inclusions in the melt create bubbles, which cavitate when the critical pressure intensity is reached. During cavitation microjets are generated locally with a speed of up to 400 m/s, pressure reaches up to 1000 atm, temperature can reach 20000 K and temperature rate 10^9 K/s. The formation of bubbles takes place around the inclusions of gases and impurities, so the cavitation threshold can be different for the same material [74]. A typical way to detect cavitation is to record an acoustic signal from the liquid region. The cavitation spectrum contains sub-harmonics and ultra-harmonics of the main frequency f which is used to excite the cavitation. Main lines in the frequency spectrum to acoustically detect cavitation are ½f and 3/2f in the frequency spectrum. During full cavitation, the signal covers the entire spectrum [30,31,77].

Abramov [44] studied cavitation in liquid metals when pressure oscillations are created mechanically, initiation of cavitation was obtained in aluminum above 550 kPa, and in tin at 280 kPa. Vives [30] has shown electromagnetic induction of cavitation using alternating current and a perpendicular static magnetic field by obtaining cavitation in aluminum at 65 kPa. Bojarevics [78] studied a two inductor system, in which one inductor is for induction heating purpose, while another is placed from the top to the melt surface, causing pressure oscillations and cavitation.

The inspiration to use combined alternating and static magnetic field for dispersion of particle agglomerates comes from the long-term cooperation with the Helmholtz-Zentrum Dresden-Rossendorf, during which the EM method for

dispersion of particle agglomerates in ODS steel was studied [7,43]. As a result of these studies, the concept to use EM methods for lower melting temperature metals has been developed – described in Chapter 3.2 and [dis5].

Fine-grain and homogeneous alloy microstructure is an important to obtain high-quality alloy with good and homogeneous mechanical properties. The impact of pulsed magnetic field (PMF) has been widely studied in the literature for microstructure improvement of an alloy during its crystallization. EM interaction leads to a finer grain and dendritic structure [34,37,79]. For example, Zhang has shown [33] an 18% improvement in tensile strength of A357 alloy after PMF treatment. Hua showed [6] the microstructure improvement in tin alloy by using combined PMF and B_{DC} magnetic field during alloy crystallization. This is only literature found where a combined effect of PMF and BDC is used. Chapter 3.3. and [dis6] describes a study of PMF exposure for particle dispersion in MMC, which has not been proposed in the literature so far. Similarly to Hua study, the effect of EM exposure on the tin alloy microstructure is also tested, however pulsed field interaction with liquid metal is explained in more detail.

The liquid phase of alloy production ends with melt crystallization. Crystallization conditions are essential in order to have a homogeneous chemical composition of the material, microstructure distribution, as well as the distribution of particles mixed in the alloy. One way to solidify an alloy in a controlled manner is with a continuous casting crystallizer, in which the metal is drawn through a region to be cooled, thus ensuring uniform crystallization conditions throughout the melt solidification. Although several types of electromagnetic stirring in continuous casting crystallizers have been studied before [80,81], in this work laboratory scale continuous casting crystallizer with EM interaction is developed. With this crystallizer it is planned to conduct research both on the effect of microstructure of the alloys and also to continue the development of MMC technology by performing their crystallization. Until now, it is not clear whether the particles will not float or agglomerate during crystallization. EM stirring could also help to solve such potential problems. The study of the developed EM exposure on the A360 alloy during its crystallization is described in chapter 3.4 and [dis7].

The task of applying EM methods for dispersion of particle agglomerates in metal can be divided into the following stages:

1) Development of an analytical and numerical model for the description of the dominant physical effects.
2) Development of the experimental system with superconducting magnet and sample preparation by powder metallurgy.
3) Experimental series by using B_{AC} and B_{DC} processing of samples.

4) Development of experimental system with pulsed magnetic field interaction.
5) Experimental series with combined PMF and B_{DC}.
6) Development of continuous casting crystallizer which is equipped with electromagnetic interaction.
7) Experimental series with continuous casting crystallizer.

3.2 EM induced cavitation for particle dispersion in MMC

3.2.1 Cavitation generation with alternating and static magnetic field

In this study, it is proposed to create pressure oscillations for cavitation by using a combination of alternating B_{AC} and static B_{DC} magnetic field (both fields are parallel). This concept was chosen because the method could also be scaled for larger melt volumes. In the experiments, a superconducting magnet up to 4 T was chosen as the B_{DC} source. A high-frequency inductor was used as the B_{AC} field source up to 0.13 mT. The maximum amplitude of the oscillating pressure can be estimated as $B_{AC}B_{DC}/\mu_0 \approx 400\ kPa$. Based on the literature review, such amplitude is sufficient to achieve cavitation in alloys.

Oscillation of small bubbles in a fluid caused by an alternating external pressure $p_\infty(t)$ can be described by the Rayleigh-Plesset equation (20), where *R(t)* is a changing bubble radius, P_0 is the constant external pressure, R_0 is the initial radius of the bubble, c is the specific heat of the gas bubble (c_p/c_v), ρ, γ, and μ are the density, surface tension, and viscosity of the liquid accordingly [25, 26].

$$R\ddot{R} + \frac{3}{2}\dot{R}^2 = \frac{1}{\rho}\left[\left(P_0 + \frac{2\gamma}{R_0}\right)\left(\frac{R_0}{R}\right)^{3c} - \frac{4\mu\dot{R}}{R} - \frac{2\gamma}{R} - p_\infty(t)\right] \qquad (20)$$

For a small bubble, which is mainly affected by surface tension, the critical pressure P_T at which cavitation will start can be determined using expression (21).

$$P_T = P_0 + \frac{4}{3}\left[\frac{3\gamma^3}{3R_0^3(P_0 + 2\gamma/R_0)}\right]^{1/2} \qquad (21)$$

If in equation (21) the ambient pressure value is around 0.5 kPa, it can be neglected in comparison with the pressure due to acoustic pressure and Laplace pressure. By knowing the aluminum surface tension 1.007 N/m, the minimum size of cavitation bubbles is estimated around 2 μm.

The alternating magnetic field causes the liquid metal flow, while the static magnetic field damps the vorticity component perpendicular to the magnetic field lines [45]. Motion damping can be described by the MHD interaction parameter (22), which in this case is at least 400. It means that the macroscopic flow in a static 4 T magnetic field is significantly damped.

$$N = \frac{\sigma B^2 R}{\rho u} \tag{22}$$

The samples in these experiments are tablets (30 mm in diameter) pressed from Al-6wt%Mg alloy or tin (Sn) and SiC particle (100 nm) powders. During the experiment, the tablet is placed on a water-cooled stand, the sample is melted in the 9-18 kHz B_{AC} field and exposed to combined B_{AC} and B_{DC} treatment. After the experiment the sample freezes on the cooling stand by reducing the intensity of the B_{AC}. The experimental system is shown in Figure 14. The experiments to be performed were limited because of the limited time for using the superconducting magnet.

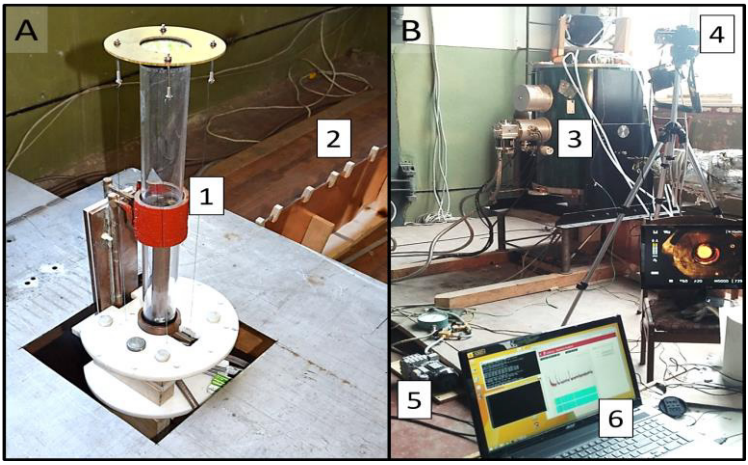

Figure 14 Experimental setup. A: sample in the inductor (1), AC current supply line (2); B: superconducting magnet (3), camera (4), vacuum pump (5), sound recording (6).

The experimental chamber is in an AC inductor, but the entire system is placed in a superconducting magnet. Piezo sensors for sound recording are glued to the cooling stand on which the MMC sample is placed. The sound spectrum could be followed up during experiments, thus immediately seeing at which moments the cavitation signal appears.

3.2.2 Results of particle dispersion experiments

The cavitation spectrum as sub and ultra-harmonics was recorded from all samples during the experiment. The cavitation signal in the experiments appeared after the alternating force intensity was changed with a delay of approximately 10-20 s. The cavitation occurred after increasing and decreasing the EM intensity. A change in the cavitation signal in response to the changes in external air pressure was also observed. In one of the experiments with tin and SiC particles, signals with many sub- and ultra-harmonics were recorded – this corresponds to full cavitation regime, see Figure 15 around second 920 of the experiment.

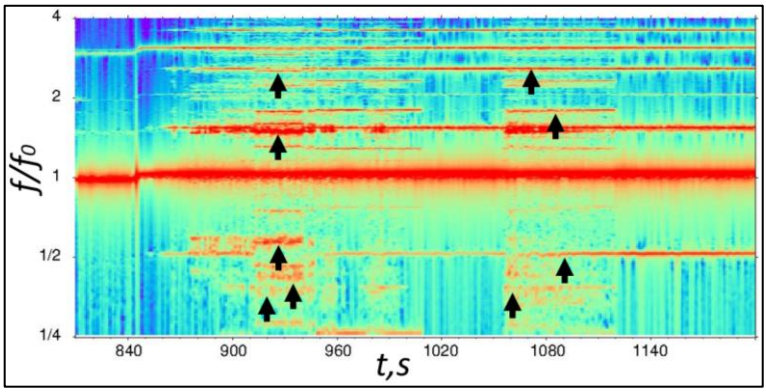

Figure 15 Sound spectrum recording from tin and SiC sample during B_{AC} and B_{DC} exposure. Arrows indicate the cavitation spectrum.

The scanning electron microscope analysis shows the particle agglomerates on the Al-Mg alloy grain boundaries, see Figure 16. On the other hand, the EDX analysis which is built in electron microscope system shows uniform distribution of particles in the grain. It is estimated that SiC is 4.2%vol in the sample - this concentration is typical for alloying alloys, which would also be the direct practical application for such a material.

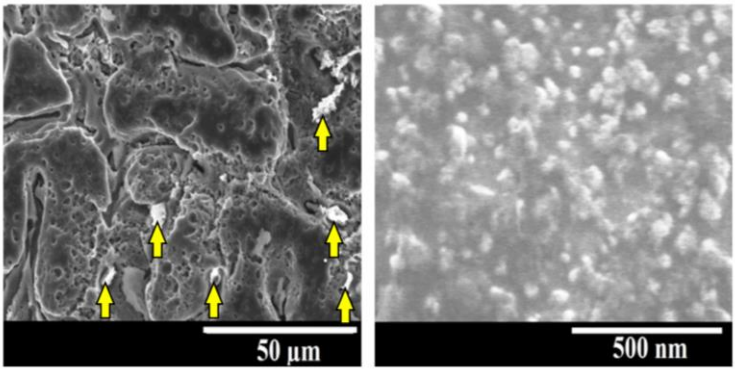

Figure 16 SiC particles in Al-Mg sample: A) Particle agglomerates on grain boundaries; B) Fully dispersed individual particles in metal grains.

The lowest electromagnetic pressure amplitude at which the cavitation signal was recorded is in tin sample at 120 kPa.

3.3 Pulsed interaction for alloy microstructure improvement

3.3.1 Development of combined pulsed and static magnetic field interaction

Since a superconducting magnet usage (as described in Chapter 3.2.) would be expensive and complicated for industrial processes, the author proposes to create similar amplitude pressure oscillations with pulsed magnetic field (PMF) and to test whether such interaction also affects particle dispersion in MMC.

Similarly to the studies described above, this time it is also proposed to use PMF in combination with the static magnetic field. The scheme of the experimental system is shown in Figure 17. The system is made axially symmetrical and consists of an electrically non-conducting graphite crucible placed in a single-turn inductor. Crucible upper diameter 95 mm, lower diameter 61 mm, height 109 mm.

The crucible and the inductor are placed in a static magnetic normal to the liquid metal region (B_{DC} = 0.46 T). The permanent magnet system is the same as used for surface wave experiments - described in Chapter 1.

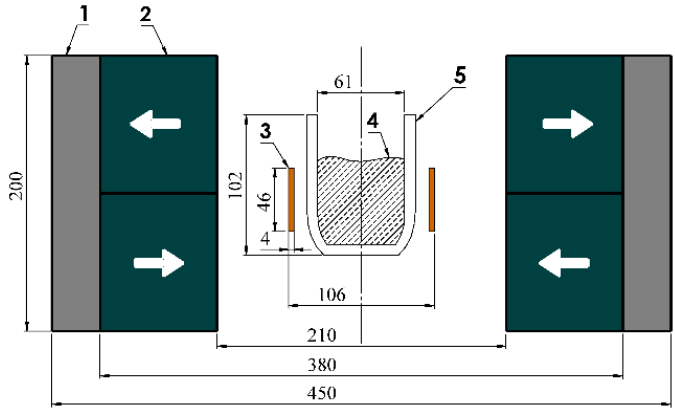

Figure 17 Schematic of the experimental system (axially symmetric). System dimensions are shown in millimeters. 1 - steel magnetic field yoke. 2 – permanent magnet system, the white arrows show the magnetization direction of the magnets. 3 – copper inductor. 4 – liquid metal. 5 – graphite crucible.

The electrical scheme for pulsed current source is shown in Figure 18 A. The inductor L is connected to the capacitor system C, which are periodically discharged through inductor. The capacitors are charged by an alternating current transformer U. A control unit with thyristor switches S controls the charging and discharging of the capacitors.

The measured peak current during the pulse discharge on the inductor supply line is 40 kA, shown in Figure 18 B. The pulse signal can be divided into its 6 characteristic stages: 1 – initial, 2 – ramp-up, 3 – top peak, 4 – ramp-down, 5 – zero cross , 6 – bottom peak. The distribution of the induced force and pressure in these stages is discussed in the publication [dis6].

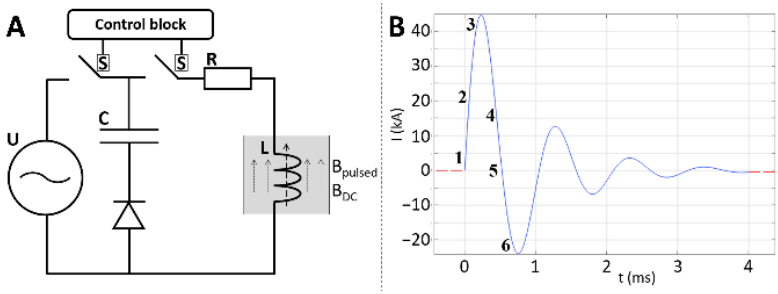

Figure 18 A: Electrical scheme of a pulsed magnetic field source. B: Measured pulsed current in coil.

The measured pulse signal can be described by the damped oscillation equation (23).

$$I = I_0 \cdot \exp(-\beta t) \cdot \sin(\omega t) \tag{23}$$

In equation $\beta = \frac{R}{2L}$ is damping coefficient, $\omega = \sqrt{\omega_0^2 - \beta^2}$ - frequency, and $\omega_0 = \frac{1}{\sqrt{LC}}$ – resonant frequency. The developed pulse system has the following parameters: C = 50 mF, U = 150 V, L= 1 μH, R = 2.4 mΩ, and I_0 = U/R = 60 kA. After substituting all the numbers into equation (23), the damped oscillation electrical signal becomes as (24).

$$I = 60000 \cdot \exp(-1200t) \cdot \sin(6000t) \tag{24}$$

Magnetic field amplitude during the pulse can be evaluated as $B_{PMF} = \frac{\mu_0 I}{2R} = 0.5$ T. Single pulse penetration of electrically conducting media is described by Grants [82]. During the experiments aluminium 6061 and tin-lead Sn-10%wt.Pb alloys are used. The pressure amplitude from the combined PMF and BDC magnetic fields gives $P = \frac{B_{PMF}(B_{DC}+B_{PMF})}{2\mu_0} = 190$ kP. If only pulsed magnetic field is used, without BDC, during the pulse generates intense liquid metal surface deformations and melt splashing. Static magnetic field damps the deformations, but significantly increase the induced force and pressure amplitude.

3.3.2 Experimental and numerical results

The induced force, pressure and surface deformations caused by EM exposure to a liquid 6061 alloy are evaluated by using program Comol Multiphysics 6.0. Figure 19 shows the magnetic field, EM force (A) and pressure (B) in the liquid aluminum skin-layer and center. For simplicity, the current in the inductor, the magnetic field, and the force or pressure are all shown on the same vertical axis.

At the beginning of the pulse, the radial component of the EM force in the skin-layer is negative, which means that the liquid metal is compressed creating a low-pressure region near the crucible wall and a high-pressure region in the center. It then oscillates around zero until the excitation from the inductor coil fades away. The pressure fluctuations in the metal during EM exposure range from -100 kPa to 150 kPa, which from the results obtained in the B_{AC} and B_{DC} experiments is to be sufficient to induce cavitation in the melt.

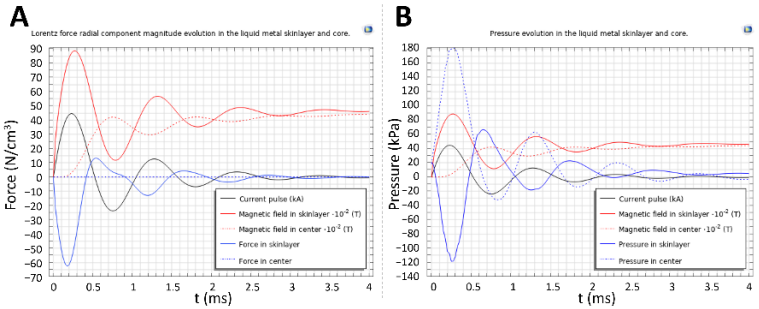

Figure 19 Graphs show electrical current in induction coil and resulting magnetic field. A: EM force in liquid metal skin layer and center. B: pressure in liquid metal skin layer and center

The numerical model was validated by comparing the free surface deformations obtained numerically and experimentally. Free surface deformations during exposure to PMF and B_{DC} show good quantitative and qualitative agreement between experiment and calculation, see [dis6] for more details.

Two types of experiments were performed. First, influence of EM exposure on the microstructure of the Sn-Pb alloy, while the alloy solidifies. Secondly, the influence of EM exposure on the distribution of TiB_2 particles in aluminum 6061 alloy, while the alloy solidifies.

A liquid Sn-10%wt.Pb alloy was overheated in a crucible 100 °C degrees above the melting point and then exposed to EM interaction. The melt solidifies in about 10 minutes. The samples were cut from the center of the longitudinal cross-section and their microstructure was compared. The average grain size in the reference samples and with only B_{DC} exposure is 220 μm, while with combined PMF and B_{DC} exposure it is 140 μm. The influence on microstructure was not observed depending on whether 1 or 3 pulses per second were used.

To examine the effect of EM exposure on particle dispersion, 2-12 μm TiB_2 particles were used. The samples were prepared by using compo-casting technique by mixing 8 wt% particles into the 6061 alloy. The alloy was overheated to 750 °C degrees and exposed to EM until solidification. Solidification takes about 5 minutes. The images obtained with an optical microscope show the improvement in particle distribution after EM exposure, shown in Figure 20. Without EM exposure, the size of particle agglomerates was up to 1 mm in diameter. Although some particles were in agglomerates after PMF and B_{DC} treatment, particle agglomerates as large as in the reference samples were not observed - the size of the largest agglomerates was below 100 μm.

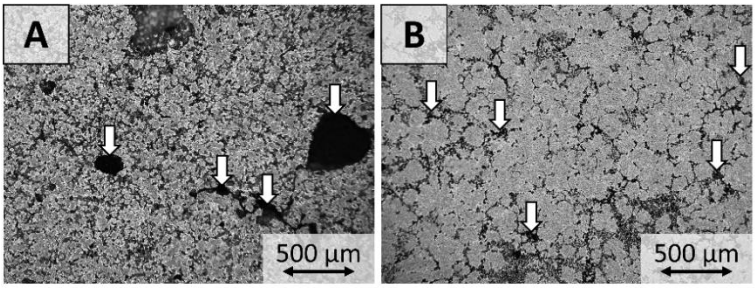

Figure 20 Optical microscope images. White arrows show particles into the alloy. A: without EM interaction, particles are in agglomerates. B: with pulsed EM processing.

The improvement in particle distribution can be influenced by two factors. First, the liquid metal is stirred for about 5 minutes during the EM exposure. Particle agglomerates are dispersed by the intense and rapid flow. Second, the induced pressure fluctuations are large enough to achieve cavitation of the liquid metal, which is a mechanism that disperses particle agglomerates. In these experiments it was not possible to capture the cavitation effect, so the mechanism which causes the particle distribution improvement is unknown.

3.4 EM interaction during alloy crystallization

3.4.1 Development of continuous casting crystallizer

This study experimentally investigates the effect on an alloy when it is crystallized in a static magnetic field and a direct current is passed through it. In this study A360 aluminum alloy, which is characterized by a dendritic structure and a wide temperature range in which the alloy is in semi-solid state before solidifying [83].

The developed experimental system provides cooling of the alloy with a water jets (direct chill casting). The schematic of the continuous casting crystallizer is shown in Figure 21 A. The temperature distribution along the symmetry axis is shown in Figure 21 B. An axially symmetric model was created in Comsol Multiphysics software.

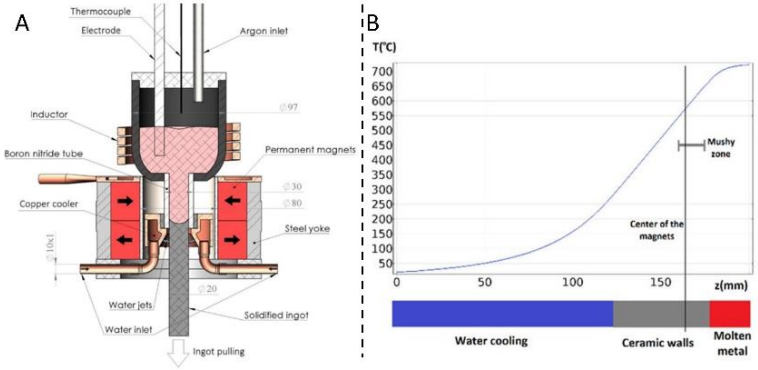

Figure 21 Schematic of crystallizer. A: Cross-section of experimental system. B: Temperature distribution along the symmetry axis.

The crystallizer was developed to produce of aluminum rods with a diameter of 12-20 mm. The magnetic field in the crystallization area is directed in the axial direction, B_{DC}=0.45 T. The permanent magnet system is conceptually similar to the system described in the surface wave and pulse exposure experiments. To provide current through the sample, the lower current electrode is attached to the rod that initiates the pulling process (seed), while the upper electrode is immersed in the liquid metal. During the experiment the metal is overheated to 700 °C with an induction coil. The crucible is covered from above with a hermetic lid and 0.25 bar argon pressure applied through tube. Applied pressure improves metal flow and overcome surface tension when the metal level in the crucible is low.

During the crystallization, an electric current of 157 A was used. For 20 mm diameter rod it corresponds to 0.5 A/mm$_2$. In the region of crystallization, the B_{DC} is parallel to the current direction, so the Lorentz force only occurs if current is diverging or converging. For the A360 alloy the temperature gradient during crystallization is 7 K/mm, which correspondingly means that the thickness of the semi-solid zone is about 3.5 mm. The values of the interaction parameter N=2000 and the Hartmann number Ha=60 shows that the inertial and viscous forces are small and the metal flow is mainly determined by the EM forces. Using the Navier-Stokes equation, the flow velocity around the dendrites can be estimated to be 0.8 mm/s, which makes the flow circle around the dendrite approximately twice per second. A more detailed description of the system can be found in [dis7].

3.4.2 Results of alloy crystallization

In the experiments, the A360 alloy solidified with velocity of 2 mm/s. After obtaining the rods, the samples were cut and analyzed with an optical microscope. Microhardness and tensile strength according to ASTM E8 standard of the samples were also determined.

Microstructure analyzes were performed on longitudinal and transverse cross-sections of rods. Without EM exposure, the alloy has a columnar microstructure. After crystallization in only static magnetic field, the longitudinal structure disappears. If the current through the metal and the B_{DC} field are used, a small-scale flow around the dendrites is obtained. Such a flow significantly increases the heat transfer between the solid and liquid phases, which results in a fine-grained homogeneous microstructure.

Before the tensile strength tests of the samples, the samples were processed according to the T6 heat treatment process. The results of tensile tests are shown in Figure 22.

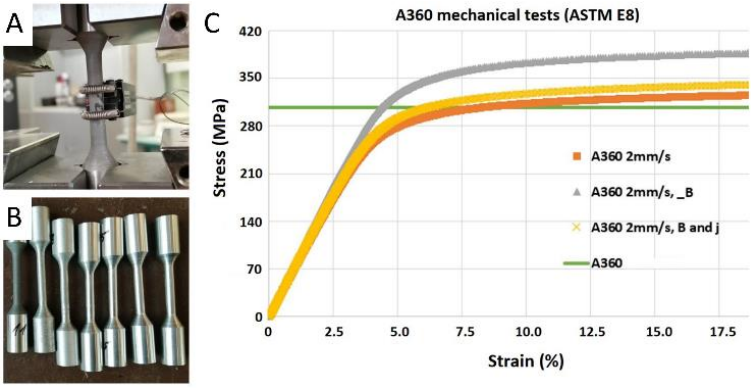

Figure 22 Tensile strength test results. A: Extension measuring sensor on the sample. B: Samples produced according to the ASTM E8 standard. C: Tensile strength measurements from various A360 samples.

The ultimate tensile strength (UTS) of A360 alloy according to the standard is 317 MPa [84]. The UTS of all samples exceeds the standard value found in the literature, see Table 3.

The rod crystallized only in the B_{DC} field showed the highest tensile strength. B_{DC} and current exposure also showed 7% higher ultimate tensile strength but lower yield strength. A more detailed analysis of the mechanical properties would require a larger volume of samples, at the same time it can be seen that the EM treatment improves the mechanical tensile strength.

Microhardness tests of all samples showed a Vickers hardness of 128 HV. A more detailed description of the results is presented in the publication [dis7]

Table 3 Mechanical properties of the samples obtained with various crystallization regimes

	A360 [84]	2mm/s	2mm/s (B_{DC}=0.4T)	2mm/s (B_{DC}=0.4T, j=0,5 A/mm^2)
Yield strength (MPa)	170	242	315	236
Young modulus (GPa)	70	70.6	71.0	70.8
Ultimate tensile strength (MPa)	317	322	395	346

3.5 Conclusions and further technology development

3.5.1 Conclusions

1. By using the B_{AC} and B_{DC} magnetic field exposure a cavitation spectrum was measured in aluminum magnesium alloy and tin samples. The lowest pressure value at which the cavitation was obtained is in tin at 120 kPa (Figure 15). It has been observed that the cavitation start is affected by:
    a. Changes in external pressure.
    b. Material chemical composition.
    c. Electromagnetic exposure intensity changes.
2. SEM and EDX analyzes show that exposure to B_{AC} and B_{DC} fields affects the particle distribution in the Al+SiC (100 nm) alloy compared to the reference samples. Particles are visible both on the grain boundaries and inside the grain (Figure 16).
3. Experimental observations show that combined pulsed and static magnetic field influence the particle distribution in MMC by partly dispersing the particle agglomerates and by making the distribution uniform.
4. Static magnetic field damps the melt surface deformation caused by pulsed magnetic field, while induced Lorentz force and pressure is significantly increased.
5. Static magnetic field in combination with current through the metal during solidification influence the alloy microstructure. Generated Lorentz force modifies the columnar microstructure to equiaxed, which results in increased alloy tensile strength

.

3.5.2 Further technology development – crystallization of MMC

For more detailed analysis of the obtained MMC materials, it is necessary to do larger series of experiments in order to quantitatively analyze the properties of the obtained materials. It is planned to make full experimental cycle for the MMC production process by electromagnetically stirring the particles into the melt, dispersing their agglomerates and solidifying the material in the crystallizer. Then samples can be analyzed by tensile strength tests and by rolling the rods into wire for additive manufacturing tests.

4 Summary and thesis

Main conclusions

In this thesis, combination of magnetic fields for practical applications in metallurgy have been studied. The combinations are proposed for three processes. According to each process new experimental systems are developed, including new EM regimes which have not been previously studied in the literature. During the studies, new and promising results were obtained for further technological development. The main achievements and conclusions of this thesis are mentioned below:

1. **On surface waves:**
   1.1. Comparing to the waves induced by an alternating magnetic field in case of combined B_{AC} and B_{DC} exposure meniscus on the surface is not formed and waves are obtained over the entire surface. Experiments show it in the dimensionless frequency range from 0.5 to 4.
   1.2. In case of both exposures B_{AC} and combination of B_{AC} and B_{DC} magnetic fields, waves are traveling toward the center when B_{AC} intensity is low.

2. **On mixing of particles into the melt to produce metal matrix composites**:
   2.1. Permanent magnet dipole stirrer can be used to generate flow in industrial scale liquid aluminium furnace and used as an stirrer.
   2.2. By using permanent magnet stirrer in combination with induction heating micro and nano size particles can be stirred into aluminium melt. The efficiency of the method depends on the used particles and alloy.

3. **On particle dispersion in metal matrix composites:**
   3.1. Cavitation can be generated in liquid metal by using alternating and static magnetic field superposition. Cavitation is confirmed by measuring cavitation sound spectrum.
   3.2. Developed combined BAC and BDC magnetic field, as well as combined Pulsed and BDC magnetic fields interactions influence the particle distribution in MMC by making it more uniform and by reducing the amount of agglomerates and their characteristic size.
   3.3. Static magnetic field damps the liquid metal surface deformations caused by pulsed magnetic field and also significantly increases induced Lorentz force and pressure amplitude.

4. **Conclusions about combined EM field systems:**
   4.1. Exposure of combined magnetic fields allows to obtain new regimes for contactless processing of the melt for practical applications.
   4.2. The number of parameters characterizing combined magnetic field systems increases significantly, compared to one field exposure, so the selection and optimization of parameters becomes more laborious.
   4.3. Permanent magnets and their assemblies can be used effectively to generate a static and alternating (up to 100 Hz) magnetic field. One of the main advantages is that powerful current supplies are not needed as it is by using electromagnets and low frequency inductors.
   4.4. During the development of combined magnetic field systems, interaction of magnetic field sources should be considered. By combining inductor and permanent magnet systems, the technical risks associated with induced currents and magnetic attraction can be reduced.

Thesis

1. Using a combination of static and alternating magnetic fields, surface waves can be generated over the entire liquid metal surface when system radius is larger than skin-layer.
2. A permanent magnet stirrer combined with induction heating can create a flow that ensures mixing of non-magnetic particles into the metal through a metallurgical route.
3. Cavitation in a liquid metal can be achieved by using the superposition of an alternating and static magnetic field.

Acknowledgements

I would like to express my deep gratitude to University of Latvia Institute of Physics MHD Technology laboratory colleagues, especially to my research supervisor Andris Bojarevičs, for the support and help during the whole study process.

I would like to thank my family, friends and, especially Linda, for the never-ending support.

References

[1] ABB, Optimised electromagnetic stirring in melting and holding furnaces, (n.d.). https://new.abb.com/metals/abb-in-metals/references/optimised-ems-in-aluminium-melting-and-holding-furnaces.

[2] W.H. Macintosh, Induction furnaces for melting secondary aluminium, Conservation & Recycling. 6 (1983) 41–48. doi:10.1016/0361-3658(83)90015-2.

[3] I. Bucenieks, High pressure and high flowrate induction pumps with permanent magnets, MAGNETOHYDRODYNAMICS. 39 (2003) 411–418.

[4] D. Buchenau, V. Galindo, S. Eckert, The magnetic flywheel flow meter: Theoretical and experimental contributions, Applied Physics Letters. 104 (2014). doi:10.1063/1.4881330.

[5] M.G. Hvasta, W.K. Nollet, M.H. Anderson, Designing moving magnet pumps for high-temperature, liquid-metal systems, Nuclear Engineering and Design. 327 (2018) 228–237. doi:10.1016/j.nucengdes.2017.11.004.

[6] J. Hua, Y. Zhang, C. Wu, Grain refinement of Sn–Pb alloy under a novel combined pulsed magnetic field during solidification, Journal of Materials Processing Technology. 211 (2011) 463–466. doi:https://doi.org/10.1016/j.jmatprotec.2010.10.023.

[7] M. Sarma, I. Grants, T. Herrmannsdörfer, G. Gerbeth, Contactless generation of cavitation in high temperature liquid metals and its impact on particle dispersion in solidified iron and steel samples, Journal of Materials Processing Technology. 291 (2021) 117041. doi:10.1016/j.jmatprotec.2021.117041.

[8] O. Budenkova, M. Milgravis, C. Garnier, A. Gagnoud, Y. Delannoy, S. Semenov, P. Chometon, S. Rivoirard, M. Alamir, J. Etay, Application of modulated calorimetry to the liquid metals using electromagnetic levitation and static magnetic field, IOP Conference Series: Materials Science and Engineering. 424 (2018) 12004. doi:10.1088/1757-899X/424/1/012004.

[9] Y. Fautrelle, A.D. Sneyd, Surface waves created by low-frequency magnetic fields, European Journal of Mechanics - B/Fluids. 24 (2005) 91–112. doi:10.1016/J.EUROMECHFLU.2004.05.005.

[10] J.M. Galpin, Y. Fautrelle, A.D. Sneyd, Parametric resonance in low-frequency magnetic stirring, Journal of Fluid Mechanics. 239 (1992) 409–427. doi:10.1017/S0022112092004464.

[11] J.M. Galpin, Y. Fautrelle, Liquid-metal flows induced by low-frequency alternating magnetic fields, Journal of Fluid Mechanics. 239 (1992) 383–408. doi:10.1017/S0022112092004452.

[12] C. Karcher, V. Minchenya, Control of free-surface instabilities during electromagnetic shaping of liquid metals, Magnetohydrodynamics. (2009) 511.
[13] A. Deng, E. Wang, Y. XU, X. Zhang, J. He, Oscillation Characteristics of Molten Metal Free Surface Under Compound Magnetic Field, Journal of Iron and Steel Research, International. 18 (2011) 25–37. doi:10.1016/S1006-706X(11)60060-5.
[14] M. Héder, From NASA to EU: the evolution of the TRL scale in Public Sector Innovation, The Innovation Journal. 22 (2017) 1–23. https://eprints.sztaki.hu/9204/.
[15] A.J. Knowles, X. Jiang, M. Galano, F. Audebert, Microstructure and mechanical properties of 6061 Al alloy based composites with SiC nanoparticles, Journal of Alloys and Compounds. 615 (2014) S401–S405. doi:10.1016/j.jallcom.2014.01.134.
[16] A. Mazahery, H. Abdizadeh, H.R. Baharvandi, Development of high-performance A356/nano-Al2O3 composites, Materials Science and Engineering: A. 518 (2009) 61–64. doi:10.1016/j.msea.2009.04.014.
[17] Y. Yang, J. Lan, X. Li, Study on bulk aluminum matrix nano-composite fabricated by ultrasonic dispersion of nano-sized SiC particles in molten aluminum alloy, Materials Science and Engineering A. 380 (2004) 378–383. doi:10.1016/j.msea.2004.03.073.
[18] A. Mussatto, I.U.I. Ahad, R.T. Mousavian, Y. Delaure, D. Brabazon, Advanced production routes for metal matrix composites, Engineering Reports. 3 (2021) e12330. doi:10.1002/eng2.12330.
[19] N. Panwar, A. Chauhan, Fabrication methods of particulate reinforced aluminium metal matrix composite - a review, Materials Today: Proceedings. 5 (2018) 5933–5939. doi:10.1016/j.matpr.2017.12.194.
[20] S. Sarkar, A. Bhirangi, J. Mathew, R. Oyyaravelu, P. Kuppan, A.S.S. Balan, Fabrication characteristics and mechanical behavior of rice husk ash-silicon carbide reinforced Al-6061 alloy matrix hybrid composite, Materials Today: Proceedings. 5 (2018) 12706–12718. doi:10.1016/j.matpr.2018.02.254.
[21] J.P. Vanam, R. Chiranjeevi, R.S. Kumar, V.V. Ramana, A.S. Kumar, Effect of SiC on Mechanical, Microstructure and Tribological properties of Aluminum MMC processed by Stir Casting, IOP Conference Series: Materials Science and Engineering. 455 (2018). doi:10.1088/1757-899X/455/1/012017.
[22] S. Sachinkumar, S. Narendranath, D. Chakradhar, Studies on microstructure and mechanical characteristics of as cast AA6061/SiC/fly ash hybrid AMCs produced by stir casting, Materials Today: Proceedings. 20 (2020) A1–A5. doi:10.1016/j.matpr.2020.01.266.
[23] P.G. Karandikar, T.W. Chou, Characterization of aluminium-matrix

composites made by compocasting and its variations, Journal of Materials Science. 26 (1991) 2573–2578. doi:10.1007/BF02387719.
[24] S.P. Dwivedi, S. Sharma, R.K. Mishra, Electromagnetic stir casting and its process parameters for the fabrication and refined the grain structure of metal matrix composites – a review, International Journal of Advance Research and Innovation. 2 (2014) 639–649. doi:10.51976/ijari.231421.
[25] A. Kumar, S. Lal, S. Kumar, Fabrication and characterization of A359/Al2O3 metal matrix composite using electromagnetic stir casting method, Journal of Materials Research and Technology. 2 (2013) 250–254. doi:10.1016/j.jmrt.2013.03.015.
[26] A. Bojarevičs, R. Baranovskis, I. Kaldre, M. Milgrāvis, T. Beinerts, Two cylinder permanent magnet stirrer for liquid metals, IOP Conference Series: Materials Science and Engineering. 228 (2017) 12022. doi:10.1088/1757-899X/228/1/012022.
[27] S. Kant, A.S. Verma, Stir casting process in particulate aluminium metal matrix composite: a review, International Journal of Mechanics and Solids. 9 (2017) 61–69.
[28] D. Zhou, F. Qiu, H. Wang, Q. Jiang, Manufacture of nano-sized particle-reinforced metal matrix composites: A review, Acta Metallurgica Sinica. 27 (2014) 798–805. doi:10.1007/s40195-014-0154-z.
[29] U. Pandey, R. Purohit, P. Agarwal, S.K. Dhakad, R.S. Rana, Effect of TiC particles on the mechanical properties of aluminium alloy metal matrix composites (MMCs), Materials Today: Proceedings. 4 (2017) 5452–5460. doi:10.1016/j.matpr.2017.05.057.
[30] C. Vivès, Crystallization of aluminium alloys in the presence of cavitation phenomena induced by a vibrating electromagnetic pressure, Journal of Crystal Growth. 158 (1996) 118–127. doi:10.1016/0022-0248(95)00344-4.
[31] I. Grants, G. Gerbeth, A. Bojarevičs, Contactless magnetic excitation of acoustic cavitation in liquid metals, Journal of Applied Physics. 117 (2015) 204901. doi:10.1063/1.4921164.
[32] Z. Zhao, Y. Liu, L. Liu, Grain Refinement Induced by a Pulsed Magnetic Field and Synchronous Solidification, Materials and Manufacturing Processes. 26 (2011) 1202–1206. doi:10.1080/10426914.2011.564251.
[33] L. Zhang, W. Zhan, F. Jin, Q. Zhou, Microstructure and properties of A357 aluminium alloy treated by pulsed magnetic field, Materials Science and Technology. 34 (2018) 698–702. doi:10.1080/02670836.2017.1410925.
[34] X. Bao, Y. Ma, S. Xing, Y. Liu, W. Shi, Effects of Pulsed Magnetic Field Melt Treatment on Grain Refinement of Al-Si-Mg-Cu-Ni Alloy Direct-Chill Casting Billet, Metals. 12 (2022). doi:10.3390/met12071080.
[35] Y. ZHAO, S. ZHANG, G. CHEN, Aluminum matrix composites

reinforced by in situ Al2O3 and Al3Zr particles fabricated via magnetochemistry reaction, Transactions of Nonferrous Metals Society of China. 20 (2010) 2129–2133. doi:https://doi.org/10.1016/S1003-6326(09)60429-5.

[36] Y.D. Yu, C.X. Li, The effect of alternative low frequency electromagnetic field on the solidification microstructure and mechanical properties of ZK60 alloys, Materials & Design. 44 (2013) 17–22. doi:https://doi.org/10.1016/j.matdes.2012.07.034.

[37] T. Campanella, C. Charbon, M. Rappaz, Grain refinement induced by electromagnetic stirring: A dendrite fragmentation criterion, Metallurgical and Materials Transactions A. 35 (2004) 3201–3210. doi:10.1007/s11661-004-0064-1.

[38] O. Zaitov, V.A. Kolchuzhin, Bitter coil design methodology for electromagnetic pulse metal processing techniques, Journal of Manufacturing Processes. 16 (2014) 551–562. doi:10.1016/j.jmapro.2014.07.008.

[39] K. Halbach, Specialty magnets, AIP Conference Proceedings. 153 (1987) 1277–1295. doi:10.1063/1.36378.

[40] A. Bojarevičs, T. Beinerts, Y. Gelfgat, I. Kaldre, Permanent magnet centrifugal pump for liquid aluminium stirring, Journal International Journal of Cast Metals Research. 29 (2016) 154–157. doi:10.1080/13640461.2015.1120998.

[41] T. Beinerts, R. Bojarevics, Andris Baranovskis, M. Milgravis, I. Kaldre, Permanent magnet dipole stirrer for aluminium furnaces, IOP Conference Series: Materials Science and Engineering. 424 (2018). doi:10.1088/1757-899X/424/1/012037.

[42] A. Bojarevics, T. Beinerts, Experiments on liquid metal flow induced by a rotating magnetic dipole, Magnetohydrodynamics. 46 (2010) 333–338.

[43] M. Sarma, I. Grants, A. Bojarevics, G. Gerbeth, Magnetically Induced Cavitation for the Dispersion of Particles in Liquid Metals BT - Metal-Matrix Composites Innovations, Advances and Applications, in: T.S. Srivatsan, Y. Zhang, J. Harrigan William C. (Eds.), Springer International Publishing, Cham, 2018: pp. 183–192. doi:10.1007/978-3-319-72853-7_12.

[44] O. V Abramov, Action of high intensity ultrasound on solidifying metal, Ultrasonics. 25 (1987) 73–82. doi:10.1016/0041-624X(87)90063-1.

[45] A. Bojarevics, T. Beinerts, I. Grants, I. Kaldre, A. Sivars, G. Gerbeth, Y. Gelfgat, Effect of superimposed DC magnetic field on an AC induction semi-levitated molten copper droplet, Magnetohydrodynamics. 51 (2015) 437–443. doi:10.22364/mhd.51.3.4.

[46] H.B. Henderson, O. Rios, Z.L. Bryan, C.P.K. Heitman, G.M. Ludtka, G. Mackiewicz-Ludtka, A.M. Melin, M. V Manuel, Magneto-Acoustic

Mixing Technology: A Novel Method of Processing Metal-Matrix Nanocomposites, Advanced Engineering Materials. 16 (2014) 1078–1082. doi:10.1002/adem.201300534.
[47] ASTM, Standard Test Methods for Tension Testing of Metallic Materials, American Society for Testing and Materials. 03.01 (n.d.). doi:10.1520/E0008_E0008M-22.
[48] V. Benda, L. Černá, PV cells and modules – State of the art, limits and trends, Heliyon. 6 (2020). doi:10.1016/j.heliyon.2020.e05666.
[49] J. jun Wu, W. hui Ma, B. Yang, Y. nian Dai, K. Morita, Boron removal from metallurgical grade silicon by oxidizing refining, Transactions of Nonferrous Metals Society of China (English Edition). 19 (2009) 463–467. doi:10.1016/S1003-6326(08)60296-4.
[50] F. Chigondo, From Metallurgical-Grade to Solar-Grade Silicon: An Overview, Silicon. 10 (2018) 789–798. doi:10.1007/s12633-016-9532-7.
[51] P.A. Davidson, An Introduction to Magnetohydrodynamics, Cambridge University Press, Cambridge, 2001. doi:DOI: 10.1017/CBO9780511626333.
[52] W. Thomson, 2. On the Motion of Free Solids through a Liquid, Proceedings of the Royal Society of Edinburgh. 7 (1872) 384–390. doi:10.1017/S037016460004222X.
[53] G. Alcalá, M. Rivero, S. Cuevas, Effect of the magnetic field orientation on the damping of liquid metal free surface waves in the processing of materials, Applied Thermal Engineering. 75 (2015) 1296–1301. doi:https://doi.org/10.1016/j.applthermaleng.2014.09.015.
[54] J. Krumiņš, Travelling magnetic field interaction with conducting media, Zinatne. (1969) 258–262.
[55] D. Terwagne, J.W.M. Bush, Tibetan singing bowls, Nonlinearity. 24 (2011) R51. doi:10.1088/0951-7715/24/8/R01.
[56] P. Garg, A. Jamwal, D. Kumar, K.K. Sadasivuni, C.M. Hussain, P. Gupta, Advance research progresses in aluminium matrix composites: manufacturing & applications, Journal of Materials Research and Technology. 8 (2019) 4924–4939. doi:10.1016/j.jmrt.2019.06.028.
[57] F. Nturanabo, L.M. Masu, J.B. Kirabira, Novel Applications of Aluminium Metal Matrix Composites, Aluminium Alloys and Composites. (2020). doi:10.5772/intechopen.86225.
[58] R.N. Rao, S. Das, Effect of SiC content and sliding speed on the wear behaviour of aluminium matrix composites, Materials & Design. 32 (2011) 1066–1071. doi:10.1016/j.matdes.2010.06.047.
[59] J.-P. Chen, L. Gu, G.-J. He, A review on conventional and nonconventional machining of SiC particle-reinforced aluminium matrix composites, Advances in Manufacturing. 8 (2020) 279–315.

doi:10.1007/s40436-020-00313-2.
[60] P. Ajay Kumar, P. Rohatgi, D. Weiss, 50 Years of Foundry-Produced Metal Matrix Composites and Future Opportunities, International Journal of Metalcasting. 14 (2020) 291–317. doi:10.1007/s40962-019-00375-4.
[61] J.J. Moses, I. Dinaharan, S.J. Sekhar, Characterization of silicon carbide particulate reinforced AA6061 aluminum alloy composites produced via stir casting, Procedia Materials Science. 5 (2014) 106–112. doi:10.1016/j.mspro.2014.07.247.
[62] W. Zhao, S.-J. Huang, Y.-J. Wu, C.-W. Kang, Particle Size and Particle Percentage Effect of AZ61/SiCp Magnesium Matrix Micro- and Nano-Composites on Their Mechanical Properties Due to Extrusion and Subsequent Annealing, Metals. 7 (2017). doi:10.3390/met7080293.
[63] I. Bucenieks, Perspectives of using rotating permanent magnets for electromagnetic induction pump design, Magnetohydrodynamics. 36 (2000) 151–156. doi:10.22364/mhd.
[64] R. Baranovskis, D. Berenis, I. Grants, A. Bojarevics, T. Beinerts, M. Milgravis, Contactless Aluminum Degassing System—GaInSn Model Experiments and Numerical Study, Journal of Sustainable Metallurgy. 7 (2021) 1899–1909. doi:10.1007/s40831-021-00459-8.
[65] K.K. Berga, D. Berenis, M. Kalvāns, I. Krastiņš, T. Beinerts, I. Grants, A. Bojarevičs, Model Experiment for Molten Metal Temperature Homogenization with Rotating Permanent Magnet, JOM. 74 (2022) 2450–2460. doi:10.1007/s11837-022-05288-y.
[66] P.K. Ghosh, S. Ray, Effect of porosity and alumina content on the high temperature mechanical properties of compocast aluminium alloy-alumina particulate composite, Journal of Materials Science. 22 (1987) 4077–4086. doi:10.1007/BF01133361.
[67] M. Vedani, E. Gariboldi, G. Silva, C. Di Gregorio, Influence of interface properties on mechanical behaviour of particle reinforced metal matrix composite, Materials Science and Technology. 10 (1994) 132–140. doi:10.1179/mst.1994.10.2.132.
[68] S. Gopalakrishnan, N. Murugan, Production and wear characterisation of AA 6061 matrix titanium carbide particulate reinforced composite by enhanced stir casting method, Composites Part B: Engineering. 43 (2012) 302–308. doi:10.1016/j.compositesb.2011.08.049.
[69] B.C. Pai, G. Ramani, R.M. Pillai, K.G. Satyanarayana, Role of magnesium in cast aluminium alloy matrix composites, Journal of Materials Science. 30 (1995) 1903–1911. doi:10.1007/BF00353012.
[70] J. Hashim, L. Looney, M.S.J. Hashmi, The enhancement of wettability of SiC particles in cast aluminium matrix composites, Journal of Materials Processing Technology. 119 (2001) 329–335.

doi:https://doi.org/10.1016/S0924-0136(01)00919-0.
[71] A. Awasthi, N. Panwar, A.S. Wadhwa, A. Chauhan, Mechanical characterization of hybrid aluminium composite - a review, Materials Today: Proceedings. 5 (2018) 27840–27844. doi:10.1016/j.matpr.2018.10.021.
[72] R. Baranovskis, M. Sarma, M. Ščepanskis, T. Beinerts, A. Gaile, S. Eckert, R. D., K. Lehmann, E.H. Thomsen, T. P., Investigation of particle dynamics and solidification in a two-phase system by neutron radiography, MAGNETOHYDRODYNAMICS. 56 (2020) 43–50. doi:10.22364/mhd.56.1.4.
[73] I. Grants, Rotating magnetic dipole-driven flows in a conducting liquid cylinder, Physics of Fluids. 33 (2021). doi:10.1063/5.0047240.
[74] P. Padhi, S.K. Kar, A Novel Route for Development of Bulk Al/SiC Metal Matrix Nanocomposites, Journal of Nanotechnology. 2011 (2011) 1–5. doi:10.1155/2011/413512.
[75] X. Li, Y. Yang, D. Weiss, Theoretical and experimental study on ultrasonic dispersion of nanoparticles for strengthening cast Aluminum Alloy A356, Metallurgical Science and Tecnology. 26 (2008) 12–20.
[76] G. Feyder, E. Kartheuser, L.R.R. Mohan, S. Rodriguez, Direct generation of ultrasound by electromagnetic radiation in metals in a magnetic field, Phys. Rev. B. 25 (1982) 7141–7156. doi:10.1103/PhysRevB.25.7141.
[77] E. Kartheuser, L.R. Ram Mohan, S. Rodriguez, Theory of electromagnetic generation of acoustic waves in metals, Advances in Physics. 35 (1986) 423–505. doi:10.1080/00018738600101931.
[78] V. Bojarevics, G.S. Djambazov, K.A. Pericleous, Contactless ultrasound generation in a crucible, Metallurgical and Materials Transactions A: Physical Metallurgy and Materials Science. 46 (2015) 2884–2892. doi:10.1007/s11661-015-2824-5.
[79] X. Ma, Y. Li, Y. Yang, Grain refinement effect of a pulsed magnetic field on as-cast superalloy K417, Journal of Materials Research. 24 (2009) 2670–2676. doi:10.1557/jmr.2009.0326.
[80] C.E.H. Tonry, V. Bojarevics, G. Djambazov, K. Pericleous, Contactless Ultrasonic Treatment in Direct Chill Casting, JOM. 72 (2020) 4082–4091. doi:10.1007/s11837-020-04370-7.
[81] I. Kaldre, Y. Fautrelle, J. Etay, A. Bojarevics, L. Buligins, Thermoelectric current and magnetic field interaction influence on the structure of directionally solidified Sn–10wt.%Pb alloy, Journal of Alloys and Compounds. 571 (2013) 50–55. doi:https://doi.org/10.1016/j.jallcom.2013.03.211.
[82] I. Grants, A. Bojarevičs, G. Gerbeth, Analytical solution for the diffusion of a capacitor discharge generated magnetic field pulse in a conductor,

AIP Advances. 6 (2016) 65014. doi:10.1063/1.4954400.
[83] M. Safari, M.M. Keikha, A. Kamarei, An investigation on semi-solid forming of A360 aluminium alloy by mechanical stirring, Proceedings of the Institution of Mechanical Engineers, Part E: Journal of Process Mechanical Engineering. 226 (2011) 205–215. doi:10.1177/0954408911411808.
[84] C.D. Clement, J. Masson, A.S. Kabir, Effects of Heat Treatment on Microstructure and Mechanical Properties of AlSi10Mg Fabricated by Selective Laser Melting Process, Journal of Manufacturing and Materials Processing. 6 (2022). doi:10.3390/jmmp6030052.